



Investigating the relationship between land alteration and the urban heat island of Seville city using multi-temporal Landsat data

Bijay Halder¹ · Alireza Karimi² · Pir Mohammad^{3,4} · Jatisankar Bandyopadhyay¹ · Robert D. Brown⁵ · Zaher Mundher Yaseen^{6,7,8}

Received: 17 March 2022 / Accepted: 15 August 2022 / Published online: 22 August 2022
© The Author(s), under exclusive licence to Springer-Verlag GmbH Austria, part of Springer Nature 2022

Abstract

Climate change and anthropogenic activities are affecting the entire earth, where urban areas are not an exception, being affected by extreme weather conditions and environmental disturbances. Urban expansion and industrial development have negatively affected the local climatic condition due to green space deficiency, soil moisture loss, soil erosion, land subsidence, high runoff, and low infiltration rate. Megacities are needed proper management and awareness for healthy ecosystem. The study investigated the properties of land alteration on the urban heat island (UHI) in the city of Seville, Spain. Earth observational Landsat 5 TM and 8 OLI/TIRS remote sensing datasets were used for generating the urban expansion and related land alteration. The study results indicate that built-up land increased by 139.2 Km² while agricultural land decreased by 104.07 Km². Open space and plantation areas also decreased by 62.33 Km² and 30.76 Km², respectively. The average temperature increase was around 0.13 °C per year between 1991 and 2021. Megacities need appropriate development, design, and supervision for sustainable urban development to avoid further UHI intensification. UHI map indicates that thermal variation increased from 2.21 °C (1991) to 3.42 °C (2021). The ecological disturbances also identified using UTFVI and the maps denoted that UTFVI values increased by 0.005 from 1991 to 2021. The present study outcomes are obliging for planners, researchers, and other participants for future evidence-based disaster planning and management.

1 Introduction

As per the united nations report, urban areas have a larger population than rural areas and are projected to reach 6.4 billion by 2050 (Mauree et al. 2018; Naboni et al. 2019).

The rapid urbanization around the world has had a considerable impact on urban environments through land use land cover (LULC) changes (Pauleit et al. 2005; Lambin and Geist 2008), disturbances in urban geometry (Sharma 2019; Narimani et al. 2022), and urban texture (Das et al.

✉ Pir Mohammad
pirmohammad291@gmail.com

Bijay Halder
halder06bijay@gmail.com

Alireza Karimi
alikal1@alum.us.es

Jatisankar Bandyopadhyay
jatib@mail.vidyasagar.ac.in

Robert D. Brown
rbrown@arch.tamu.edu

Zaher Mundher Yaseen
yaseen@alayan.edu.iq

¹ Department of Remote Sensing and GIS, Vidyasagar University, Midnapore- 721102, India

² Instituto Universitario de Arquitectura y Ciencias de la Construcción, Escuela Técnica Superior de Arquitectura, Universidad de Sevilla, Sevilla-41012, Seville, Spain

³ Department of Earth Sciences, Indian Institute of Technology, Roorkee Uttarakhand-247667, India

⁴ Department of Land Surveying and Geo-Informatics, The Hong Kong Polytechnic University, Kowloon, Hong Kong

⁵ Department of Landscape Architecture and Urban Planning, College of Architecture, Texas A&M University, College Station, TX 77840, USA

⁶ Department of Earth Sciences and Environment, Faculty of Science and Technology, Universiti Kebangsaan Malaysia, 43600 Bangi, Selangor, Malaysia

⁷ Adjunct Research Fellow, USQ's Advanced Data Analytics Research Group, School of Mathematics Physics and Computing, University of Southern Queensland, Toowoomba, QLD 4350, Australia

⁸ New Era and Development in Civil Engineering Research Group, Scientific Research Center, Al-Ayen University, Thi-Qar 64001, Nasiriyah, Iraq

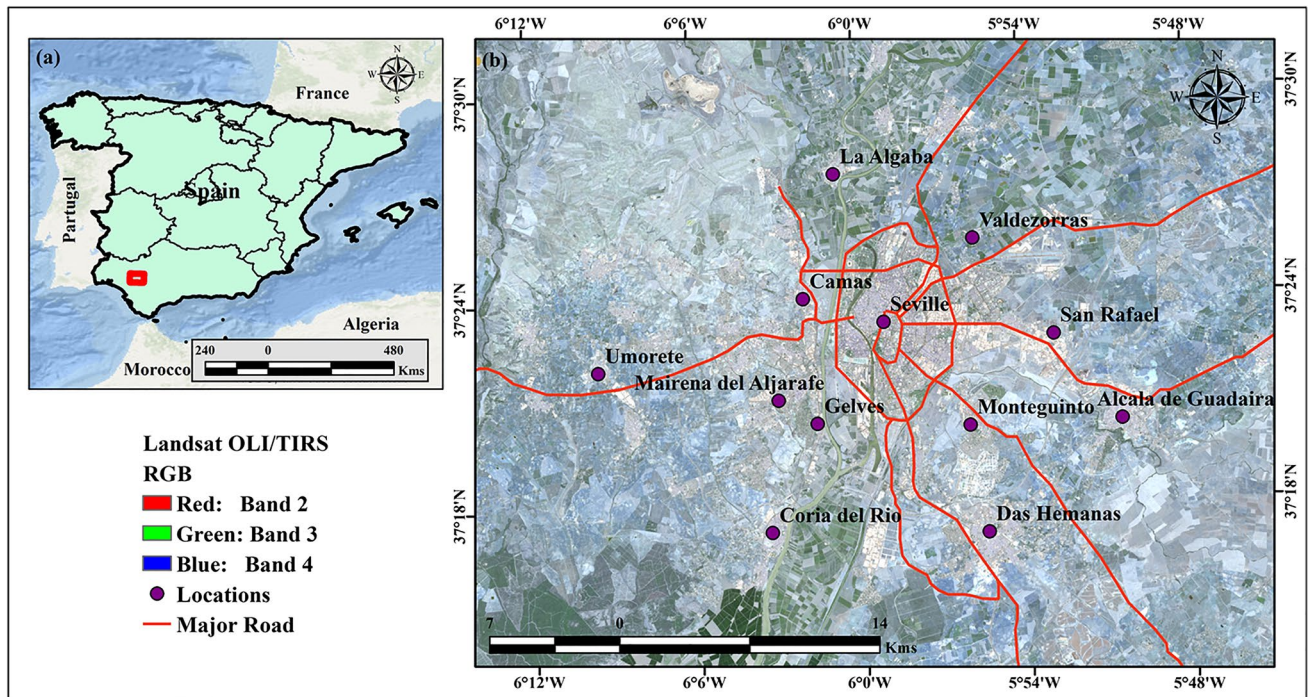


Fig. 1 Locational map of the study area

2020; Galli et al. 2021), especially in developing countries (Zhao et al. 2006). This leads to thermal variation using land surface temperature (LST) (Weng 2001; Wang et al. 2018; Lamine et al. 2018; Faqe Ibrahim 2017), earth

surface emissivity (Du et al. 2020), and vegetation cover (Ifatimehin and Ufuah 2006). In the last decades, the surface temperature was increased by around 0.87 °C due to global climate change and anthropogenic activities (Wang

Fig. 2 Adopted methodology of the study

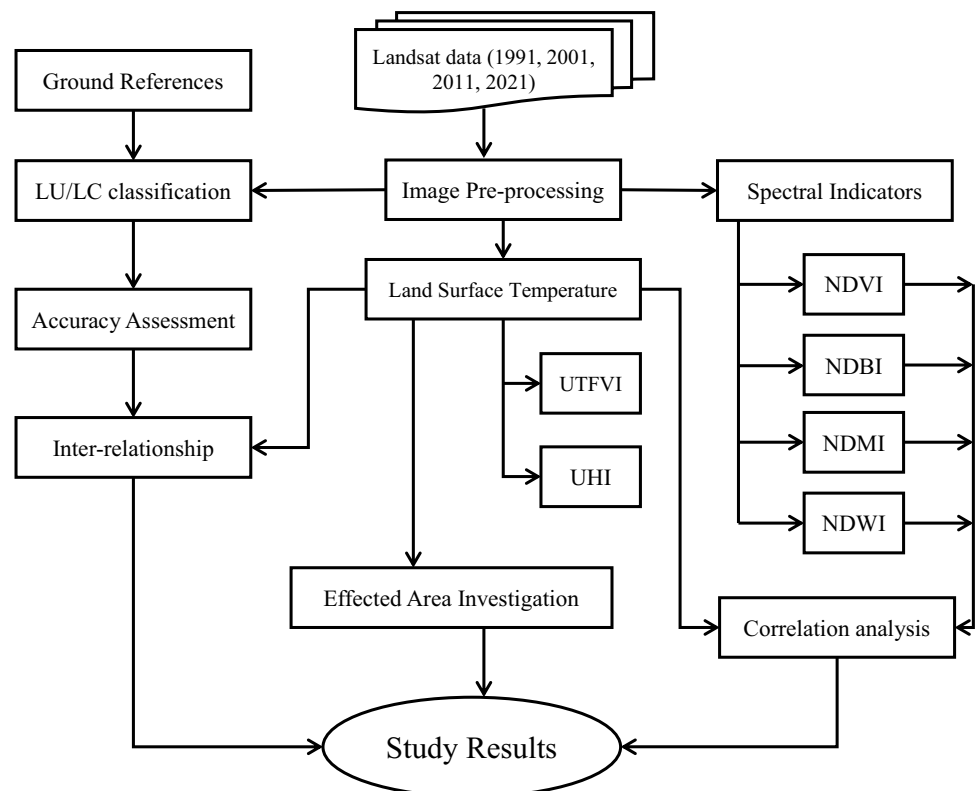


Table 1 Details of data acquisition date, satellite, and data source

Satellite	Sensor	Date	Path and row	Data source	Cloud cover
Landsat 5	TM	13–08-1991	202, 034	https://earthexplorer.usgs.gov/	<5.00
		08–08-2001	202, 034		<5.00
		04–08-2011	202, 034		<5.00
Landsat 8	OLI/TIRS	30–07-2021	202, 034		<5.00

et al. 2019; Sanikhani et al. 2019; Naganna et al. 2020; Mehr and Akdegirmen 2021) and evidence proved LST worldwide in urban areas will increase further in the future (Faqe Ibrahim 2017; Mukherjee & Singh 2020; Bayatvarkeshi et al. 2021). Increased heat storage capacity at the urban level due to the overgrowth of urban life has led to the emergence of the UHIs occurrence (Wong & Chen 2008; Karimi et al. 2020; Santos et al. 2021; Halder et al. 2021c) where urban areas are more temperate rather than the rural and fringe areas (Oke 1982).

The difference in temperature has shown a considerable effects on reduced air quality (Fallmann et al. 2016; Henao et al. 2020; Halder et al. 2021b), vegetation dynamics (Ashrafzadeh et al. 2019; Salman et al. 2021), outdoor thermal comfort (Afsharzadeh et al. 2021; Mohammad et al. 2021; Kisi et al. 2019), increased energy or dynamism consumption (Hirano & Fujita 2012; Li et al. 2019), loss of biological control (Yang et al. 2016; Halder et al. 2021a), variation in local wind patterns (Saha et al. 2021), groundwater potential area (Armanuos et al. 2021; Halder and Bandyopadhyay 2022; Ali et al. 2020), water quality (Khaleefa and Kamel 2021; Mohtar et al. 2019), developed new health emergencies like asthma, lung cancer, respiratory track infraction (Shahmohamadi et al. 2011), and many more in connection with the environment. Characteristics of UHIs are included in three major classifications including canopy layer UHI (CLUHI), surface urban heat island (SUHI), and boundary layer UHI for mesoscale examination (BLUHI) (Goswami et al. 2016; Karimi et al. 2021), given that surface and urban heat islands (SUHIs) have been proposed to investigate the spatio-temporal relationship between built-up growth with the SUHI model (Meftahi et al. 2022) and are widely used to monitor thermal variation due to geothermal observation data sets (Landsat, MODIS, and Sentinel-3) in urban areas (Milesi & Churkina 2020). Hence, examining the spatial pattern of UHI on how LULC is distributed and its effect on LST has always been one of the most important challenges for researchers. In this regard, Veena et al. (2020) investigated the UHI and thermal variation in Indian cities and noted that the temperature has been increased around 2 to 6 °C in the Indian cities. In another study (Chatterjee & Gupta 2021), the authors suggested that rises in the LST pattern are considered to be spatially associated with those areas where the intensity of land-use change

is maximum. The same results is proposed in Sarif et al. (2020); the authors recommended that the average of LST has a great impact on the distance from the city where, by decreasing and increasing, the values of LST change. In addition, Abulibdeh (2021) conducted the field survey in urban areas where climatic variation of in cities like the semi-arid Gulf region and noted that the transformation in temperature varies between 1 and 2 °C in barren land, bare land, and built-up areas. Furthermore, various studies have been conducted in Asia (Bokaie et al. 2016; Pramanik & Punia 2019; Abulibdeh 2021; Gohain et al. 2021; Karimi et al. 2021; Khan et al. 2022), Europe (Avram et al. 2019; Atasoy 2020), and the Americas (Coseo & Larsen 2014; Kulawardhana et al. 2021) that emphasized the relationship between thermal variation and land alteration and its consequences on UHIs. In addition, several studies have examined the urban sprawl impacts on UHI which is calculated normalized difference vegetation index (NDVI) (Senay et al. 2011; Chakraborty et al. 2020), normalized difference built-up index (NDBI) (Liu & Zhang 2011; Guha et al. 2018), normalized difference moisture index (NDMI) (Alibakhshi et al. 2020), and soil-adjusted vegetation index (SAVI) (Balçik 2014; Padmanaban et al. 2019).

Seville city is the mostly urbanized city where expansions of built-up and industrial areas are gradually increased due to population and anthropogenic activities. The urban areas of Seville city mainly expanded towards east, southwest, and north side, where agricultural lands are degreased due to land crisis (Ruiz-Pérez et al. 2021). Some adaptation policies are more important to protect the city, otherwise Seville city has been affected by several extreme climatic condition. The thermal remote sensing is widely used for monitoring the UHI affects and urban growth modeling using GIS, machine learning algorithm, and

Table 2 Scale of kappa coefficient

Sl no	Value of K	Strength of agreement
1	<0.20	Poor
2	0.21–0.40	Fair
3	0.41–0.60	Moderate
4	0.61–0.80	Good
5	0.81–1.00	Very good

statistical regression modeling and landscape relationships and research is capable of providing significant feedback to policymakers and researchers (Coseo & Larsen 2014; Rotem-Mindali et al. 2015; Tran et al., 2017; Mohammad et al. 2019; Falah et al. 2020). These results are usually obtained from remote sensing data, which is enough foundations of information for determining UHIs (Feyisa et al. 2014; Wu et al. 2014; Tran et al. 2017). The thermal remote

sensing datasets are widely used for urban development and investigating the land surface temperature, temperature condition index (TCI), urban thermal field variation index, and UHI studies, which is Landsat, ASTER, MODIS, and Sentinel-3 (Feng et al. 2014). Based on this availability of data, the goal of this study was to investigate land alteration, LST variation, and information related to UHIs in the city of Seville, Spain.

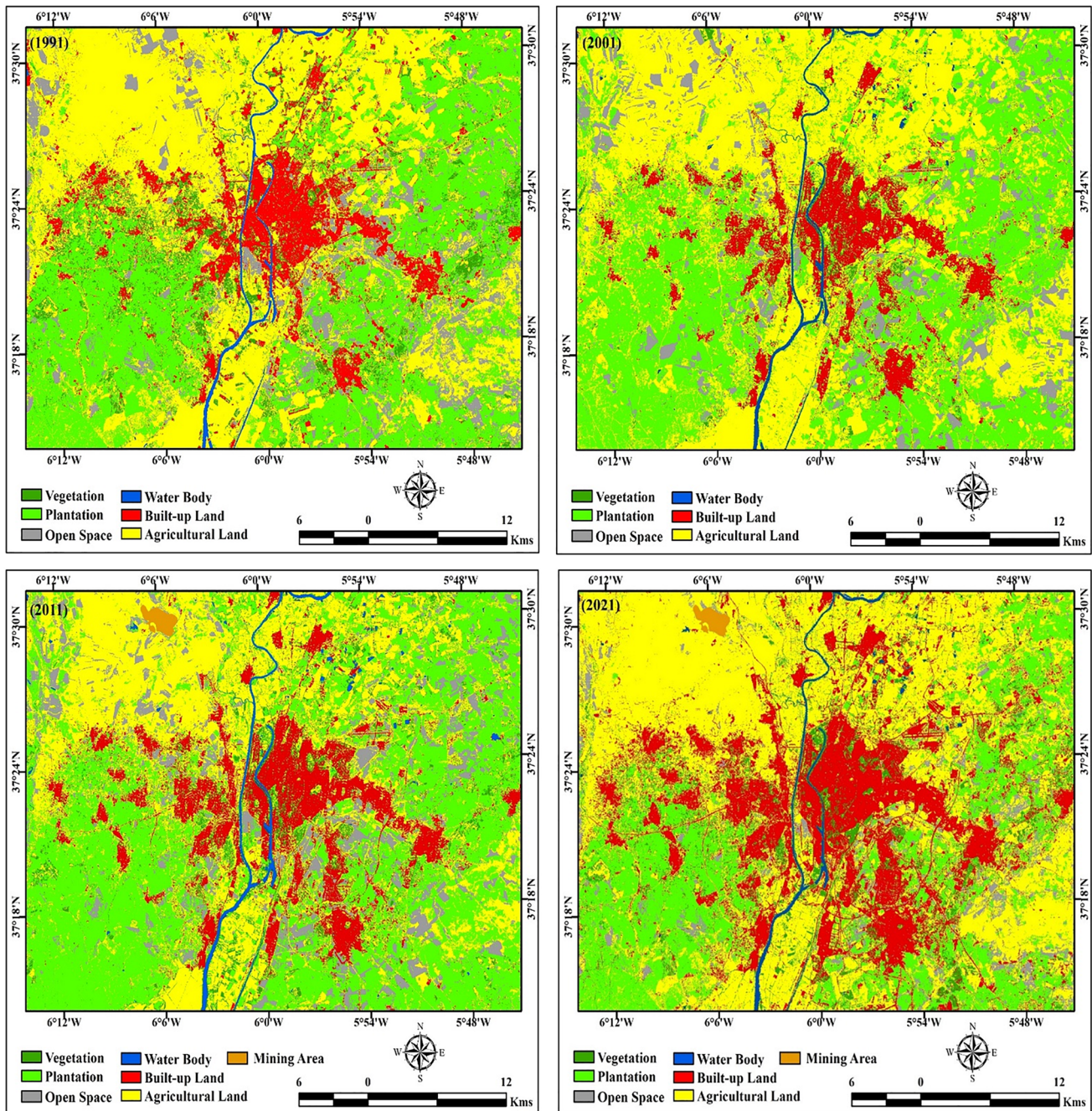


Fig. 3 Satellite image classification from 1991 to 2021

Table 4 Area calculation of LULC classification

Sl. no	Class name	Area (Sq.km)				Area (%)			
		1991	2001	2011	2021	1991	2001	2011	2021
1	Vegetation	106.83	119.23	130.65	156.88	7.38	8.24	9.03	10.84
2	Plantation	444.97	479.31	446.15	414.21	30.76	33.13	30.81	28.63
3	Open space	121.92	103.49	101.37	59.59	8.43	7.15	7.01	4.12
4	Water body	14.04	15.37	17.06	17.87	0.97	1.06	1.18	1.23
5	Built-up land	136.71	164.97	193.41	275.91	9.45	11.4	13.37	19.07
6	Agricultural land	622.24	564.34	554.13	518.17	43.01	39.01	38.3	35.82
7	Mining area	0	0	3.94	4.08	0	0	0.27	0.28

2 Study area

The case study location of Seville city is Spain which is used for land alteration, thermal variation, and UHI effects study with the location of 37.3891° N, 5.9845° W (Castillo-Manzano et al. 2015), as shown in Fig. 1. Around 690,000 people live in the Seville city of Spain. The total study area is covered around 1446.76 Km². Based on Köppen climatic classification, the study area belongs to the Csa climate with mild winters and blazing hot summers. The city has a regular annual temperature variation of 18 °C and the precipitation is about 554 mm annually. The winter months are much rainier than the summer months (Farina 2012). The total area of this study is 1447 Km² (Fig. 1). The urban design of the city of Seville shows an ecological design with a central urban area and radioactive growth, in which recently disintegrated areas are slowly incorporated (Herrera-Gomez et al. 2017).

The total green area of Seville is 890 hectares, which is mostly a green circle around the city and is not close enough to the population (de Medio Ambiente and de Territorio 2003). The Seville city is situated in the Guadalquivir valley along the bank of Guadalquivir River. The average elevation of the study area is 6 m above the sea level. In the last 30 years, Seville city has seen much investment in infrastructural development and industrial works. The current industrial and infrastructural development are influencing the local climatic diversity where thermal heat variation is the main research point to identifying the heat island related activities. Anthropogenic activities are the main reason for thermal variation where green space dynamics and unexpected population pressure are more influencing factor. Therefore, the land use and land cover change study, thermal variation, geo-spatial indicators like NDVI, NDBI, NDMI, and NDWI are used for environmental variation analysis, and UTFVI and UHI are used for surface heat island investigation.

3 Materials and methods

3.1 Data acquisition and pre-processing of Landsat data

In this study, multi-temporal Landsat 5 TM and Landsat 8 OLI/TIRS data were used for investigating the land alteration, thermal variation, and UHI study, which is derived from USGS website (<https://earthexplorer.usgs.gov/>), were utilized for land use and land cover (LU/LC), and change detection analysis, preparation of different geo-spatial indices, and estimation of LST, UTFVI, and UHI maps (Fig. 2). Four different Landsat images of the city of Seville (path/row: 202/034) were downloaded from 1991 to 2021 at a decadal interval. Table 1 is indicating the data details and acquisition data of the Landsat data. The study used three Landsat 5 TM imageries (1991, 2001, and 2011) and one Landsat 8 OLI/TIRS images (2021). Clouds have substantially impacted the LST data calculated from Landsat band 6 (TM) and Band 10 (TIRS) (Wan 1996; Ermida et al. 2020; Sekertekin and Bonafoni 2020). Therefore, the images were selected with the least cloud coverage and similar time period, which will lower the atmospheric and seasonal effect of LST in our analysis (Emran et al. 2018).

Table 3 Scale of UTFVI and level of ecological variation

Urban thermal field variation index	Urban thermal island phenomenon	Ecological evaluation index
<0	None	Excellent
0–0.005	Weak	Good
0.005–0.010	Middle	Normal
0.010–0.015	Strong	Bad
0.015–0.020	Stronger	Worse
>0.020	Strongest	Worst

Table 5 Loss and gain analysis of the LULC classification

Sl. no	Class name	Area (Sq.km)			
		(1991–2001)	(2001–2011)	(2011–2021)	(1991–2021)
1	Vegetation	12.4	11.42	26.23	50.05
2	Plantation	34.34	–33.16	–31.94	–30.76
3	Open space	–18.43	–2.12	–41.78	–62.33
4	Water body	1.33	1.69	0.81	3.83
5	Built-up land	28.26	28.44	82.5	139.2
6	Agricultural land	–57.9	–10.21	–35.96	–104.07
7	Mining area	0	3.94	0.14	4.08

Landsat data sets were processed with the help of two remote sensing-based software like ERDAS Imagine v2014 and ArcGIS v10.8. First, atmospheric corrected was done using the Fast Line-of-Sight Atmospheric Analysis of Hypercubes (FLAASH) atmospheric correction method and tool. Separated bands were layer-stacked, mosaic, and clipped from the multi-band images of Landsat 5 (TM) and Landsat 8 (OLI/TIRS) images.

3.2 LULC classification and change detection

Image classification is the technique most frequently used in GIS in which the pixel of remote sensing data is classified into different land use and land cover classes. Land use mentions to those parts of the land in which the functional role of human intervention is present for varying socioeconomic activities, whereas land cover denotes to the natural aspects of the surface of the Earth such as water bodies, vegetation, soil, and other physical parts of the earth. Since the 1960s, several techniques and methods have been developed for LULC classification for various types of satellite imagery (Phiri & Morgenroth 2017). Supervised maximum likelihood classifier (MLC), K-mean clustering, and recently developed random forest (RF), artificial neural network (ANN), deep learning techniques, fuzzy logic, etc. are the most common approaches

to classify remote sensing data (Talukdar et al. 2020). This study conducted based on a supervised image classification technique for pixel-based LULC classification using the maximum likelihood method. The study area has been classified into six different land use and land cover classes, namely vegetation, plantations, open space, water bodies, agricultural land, and built-up land. Furthermore, a change detection technique was also employed in this study using ERDAS Imagine v2014 software to understand the spatial variability of LULC classes during 1991–2021.

3.3 Accuracy assessment and kappa coefficient

Investigating the accuracy of classification map is a post-classification step and is an essential factor after classification for evaluating how accurately the LULC maps are classified (Cohen 1968). In this step, the classified LULC map from remote sensing satellite imagery is compared with the ground-truth observation. The ground-truth observation points were collected from high-resolution Google Earth data with 5 m resolution. Around 100 classifications randomly point were produced for each LULC class, and each random ground-truth sample data was collected for the classified LULC map to estimate the overall accuracy. The LULC image classification result was constructed exhausting overall accuracy (OA) and

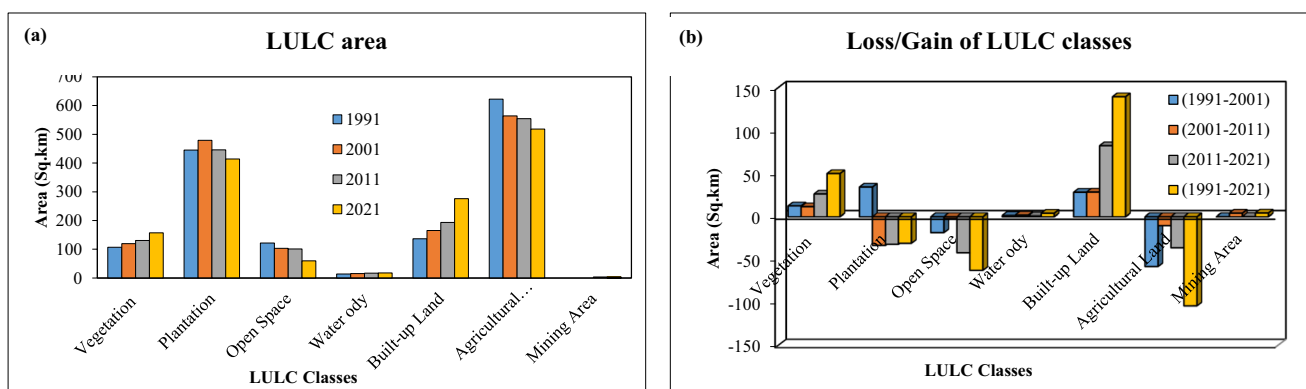


Fig. 4 Area calculation of each LULC classes. **a** Total area of different time and **b** loss and gain of the different LULC classes

Table 6 Accuracy assessment and kappa coefficient of the classification map, 1991

Class name	Ground truth/reference						Row total	Commission error	User accuracy
	Vegetation	Plantation	Open space	Water body	Built-up land	Agricultural land			
Vegetation	78	2	11	4	2	5	102	23.53%	76.47%
Plantation	3	55	5	2	4	1	70	21.43%	78.57%
Open space	5	0	42	3	1	4	55	23.64%	76.36%
Water body	7	1	18	112	2	7	147	23.81%	76.19%
Built-up land	1	2	1	2	19	0	25	24.00%	76.00%
Agricultural land	7	0	4	2	0	38	51	25.49%	74.51%
Column total	101	60	81	125	28	55	450		
Omission error	22.77%	8.33%	48.15%	10.40%	32.14%	30.91%			
Produce accuracy	77.23%	91.67%	51.85%	89.60%	67.86%	69.09%			
Overall accuracy	76.44%				Kappa coefficient	0.71			

kappa coefficient (K_i), which is a non-parametric Kappa coefficient test was used for overall classification accuracy (Table 2), as shown in Eqs. (1) and (2) below.

$$OA = \left(\frac{\sum_{i=1}^k n_{ij}}{n} \right) \tag{1}$$

$$K_i = \frac{(Observed\ accuracy - Change\ accuracy)}{(1 - Change\ accuracy)} \tag{2}$$

where, n_{ij} is the diagonal fundamentals of the error matrix, total number of LULC classes is represented by k , and n is the total number of samples in the error matrix.

3.4 Estimation of different land use indices

In this study, four different indices associated with change in land use were estimated: normalized difference vegetation index (NDVI), normalized difference built-up index (NDBI), normalized difference moisture index (NDMI), and normalized difference water index (NDWI).

Among built-up indices, the NDBI is widely used for investigating the information about built-up land in an urbanized area. It reflects the density of built-up area of a urban regions (Zha et al. 2003). It is derived using the surface reflectance of SWIR1 and NIR band (ρ_{SWIR1} and ρ_{NIR}) of Landsat 5 TM (bands 5 and 4) and Landsat 8 OLI/

Table 7 Accuracy assessment and kappa coefficient of the classification map, 2001

Class name	Ground truth/reference						Row total	Commission error	User accuracy
	Vegetation	Plantation	Open space	Water body	Built-up land	Agricultural land			
Vegetation	76	2	9	4	1	3	95	20.00%	80.00%
Plantation	3	42	2	1	3	2	53	20.75%	79.25%
Open space	5	0	59	3	1	4	72	18.06%	81.94%
Water body	7	2	16	127	2	7	161	21.12%	78.88%
Built-up land	1	2	1	2	17	0	23	26.09%	73.91%
Agricultural land	3	1	4	0	0	38	46	17.39%	82.61%
Column total	95	49	91	137	24	54	450		
Omission error	20.00%	14.29%	35.16%	7.30%	29.17%	29.63%			
Produce accuracy	80.00%	85.71%	64.84%	92.70%	70.83%	70.37%			
Overall accuracy	79.78%				Kappa coefficient	0.74			

Table 8 Accuracy assessment and kappa coefficient of the classification map, 2011

Class name	Ground truth/reference							Row total	Commission error	User accuracy
	Vegetation	Plantation	Open space	Water body	Mining area	Built-up land	Agricultural land			
Vegetation	112	10	9	2	0	2	4	139	19.42%	80.58%
Plantation	8	95	15	0	0	7	6	131	27.48%	72.52%
Open space	6	17	204	2	1	11	5	246	17.07%	82.93%
Water body	0	0	2	34	5	1	2	44	22.73%	77.27%
Mining area	0	1	1	5	29	1	2	39	25.64%	74.36%
Built-up land	2	8	4	3	1	75	3	96	21.88%	78.13%
Agricultural land	11	7	18	4	4	8	218	270	19.26%	80.74%
Column total	139	138	253	50	40	105	240	965		
Omission error	19.42%	31.16%	19.37%	32.00%	27.50%	28.57%	9.17%			
Produce accuracy	80.58%	68.84%	80.63%	68.00%	72.50%	71.43%	90.83%			
Overall accuracy	79.48%					0.75				
										Kappa coefficient

Table 9 Accuracy assessment and kappa coefficient of the classification map, 2021

Class name	Ground truth/reference							Row total	Commission error	User accuracy
	Vegetation	Plantation	Open space	Water body	Mining area	Built-up land	Agricultural land			
Vegetation	52	7	3	1	0	4	2	69	24.64%	75.36%
Plantation	4	59	9	1	2	4	4	83	28.92%	71.08%
Open space	3	8	175	0	1	7	4	198	11.62%	88.38%
Water body	1	0	3	29	8	2	2	45	35.56%	64.44%
Mining area	0	1	1	4	34	1	2	43	20.93%	79.07%
Built-up land	1	2	14	1	0	164	8	190	13.68%	86.32%
Agricultural land	5	2	11	1	0	4	275	298	7.72%	92.28%
Column total	66	79	216	37	45	186	297	926		
Omission error	21.21%	25.32%	18.98%	21.62%	24.44%	11.83%	7.41%			
Produce accuracy	78.79%	74.68%	81.02%	78.38%	75.56%	88.17%	92.59%			
Overall accuracy	85.10%					0.81				
										Kappa coefficient

TIRS satellite sensor (bands 6 and 5) by following Eq. (3) (Zha et al. 2003):

$$NDBI = \frac{(\rho_{SWIR1} - \rho_{NIR})}{(\rho_{SWIR1} + \rho_{NIR})} \tag{3}$$

For analyzing the vegetation cover, NDVI is the most useful index for calculating the vegetation density. The NIR and RED bands surface reflectance data were used for monitoring the NDVI maps (ρ_{NIR} and ρ_{RED}) of Landsat 5 TM (bands 4 and 3) and Landsat 8 OLI/TIRS satellite sensor (bands 5 and 4) by following Eq. (4) (Estoque et al. 2017):

$$NDVI = \frac{(\rho_{NIR} - \rho_{Red})}{(\rho_{NIR} + \rho_{Red})} \tag{4}$$

NDWI is used to extract the water body of an area and is superior in delineating water body compared to other available water index. The GREEN and NIR bands surface reflectance values are used for monitoring NDWI values of Seville city (ρ_{GREEN} and ρ_{NIR}) of Landsat 5 TM (bands

2 and 4) and Landsat 8 OLI/TIRS satellite sensor (bands 3 and 5) by following Eq. (5) (Xu 2006):

$$MNDWI = \frac{(\rho_{GREEN} - \rho_{NIR})}{(\rho_{GREEN} + \rho_{NIR})} \tag{5}$$

The moisture contact information of a surface is well extracted by NDMI index. The GREEN and NIR bands surface reflectance values are used for monitoring NDWI values of Seville city (ρ_{NIR} and ρ_{SWIR1}) of Landsat 5 TM (bands 2 and 4) and Landsat 8 OLI/TIRS satellite sensor (bands 3 and 5) by following Eq. (6) (Gao 1996):

$$NDMI = \frac{(\rho_{NIR} - \rho_{SWIR1})}{(\rho_{NIR} + \rho_{SWIR1})} \tag{6}$$

3.5 Land surface temperature (LST) estimation

LSTs are an essential character in understanding the thermal atmosphere and earth's surface of any urbanized area. In this

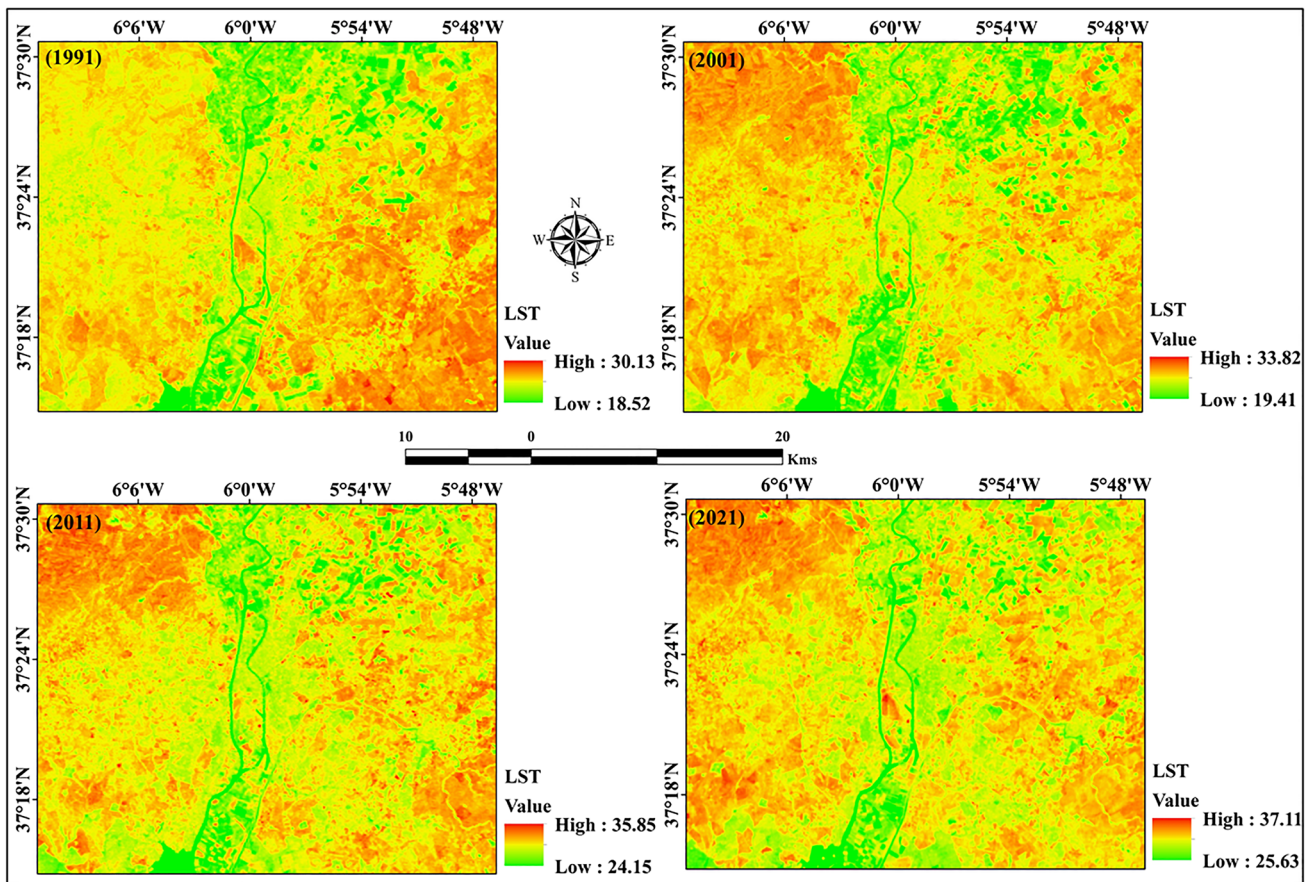


Fig. 5 Land surface temperature maps of the study area

study, the Landsat-5 TM band 6 (1991, 2001, and 2011) and Landsat-8 TIRS band 10 (2021) satellite datasets were used to generate the LST of Seville city. Landsat-8 consists of two different thermal bands (10 and 11), but due to uncertainty of the band 11 for LST estimation arising due to tilt of the orbit (Barsi et al. 2014; USGS 2017), it is not considered in this study and only band 10 is used for generation of LST images over the Sevilla city.

3.5.1 LST estimation from Landsat 5 TM

Transformation of the digital numbers (DN) of thermal band of Landsat 5 TM sensor into radiance luminance (R_{TM6}) using Eq. (7) is the initial step for the LST calculation (José A. Sobrino et al. 2004).

$$R_{TM6} = \frac{V}{255}(R_{max} - R_{min}) + R_{min} \tag{7}$$

where, V denotes the DN of the thermal band 6 of Landsat 5 TM, R_{max} indicates the 1.896 ($m.W.cm^{-2}.sr^{-1}$), and R_{min} denotes 0.1534 ($m.W.cm^{-2}.sr^{-1}$). Then the next step is to convert the radiance luminance into LST in Kelvin using Eq. (8):

$$T_k = \frac{K_1}{\ln\left(\frac{K_2}{R_{TM6}/b} + 1\right)} \tag{8}$$

and K_2 are represented the pre-calibration constant obtained from the satellite metadata file (K_1 denotes 1260.56K and K_2 indicates 607.66 $m.W.cm^{-2}.sr^{-1}.\mu m^{-1}$); b is the spectral range ($b = 1.239 \mu m$). The final LST was obtained in degrees Celsius using Eq. (9):

$$LST = T_k - 273.15 \tag{9}$$

3.5.2 LST estimation from Landsat 8 TIRS

In preparation of LST maps from Landsat 8 TIRS sensor, the step is the conversion of DNs of ground-based substances to spectral radiance using Eq. (10) (USGS 2019).

$$L_\lambda = \frac{L_{max} - L_{min}}{Qcal_{max} - Qcal_{min}} * (DN - Qcal_{min}) + L_{min} \tag{10}$$

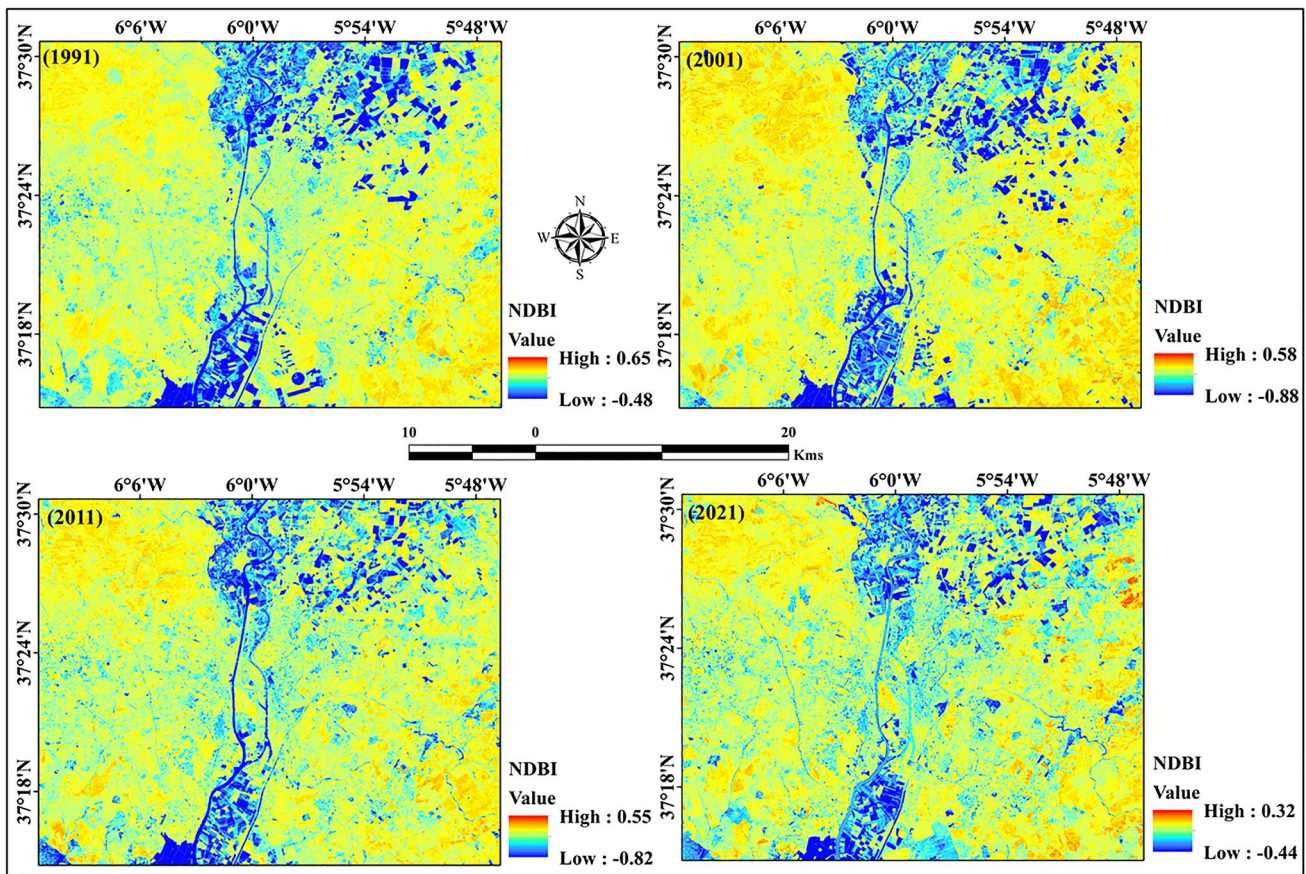


Fig. 6 NDBI maps of the study area

where, L_λ is representing the top-of-atmosphere (TOA) spectral radiance values which is measured in $W / (m^2.sr.\mu m)$, $Qcal$ is represented the quantized calibrated pixel value in digital number (DN), L_{min} and L_{max} are monitored values of the minimum and maximum spectral radiance that is scaled to $Qcal_{min}$ and $Qcal_{max}$ respectively, represent in $W/(m^2.sr.\mu m)$, where $Qcal_{min}$ and $Qcal_{max}$ indicate the minimum and maximum quantized calibrated pixel value (corresponding to L_{max}) in $DN = 255$.

The estimated radiance map from Eq. (10) is used to calculate the brightness temperature map considering the concept of black body radiation as shown in Eq. (11). (USGS 2019).

$$T_B = \frac{K_2}{\ln\left(\frac{K_1}{L_\lambda} + 1\right)} - 273.15 \tag{11}$$

where, T_B is representing the effective satellite brightness temperature, which denotes in degree Celsius, L_λ indicates the spectral radiance, and K_1 and K_2 denote the pre-calibration constant obtained from the satellite metadata file.

The following step is required for surface emissivity correction to the brightness temperature before obtaining the final LST map. In this study, the reported method by Sobrino et al. (2004) was considered which includes the estimation of standard deviation (m), combined soil and vegetation emissivity's (n), and proportion of vegetation (P_V) as calculated from Eqs. (12) to (14). These three parameters are used to obtain the final surface emissivity from Eq. (15).

$$m = (\epsilon_v - \epsilon_s) - (1 - \epsilon_s)F\epsilon_v \tag{12}$$

$$n = (\epsilon_v - \epsilon_s) - (1 - \epsilon_s)F\epsilon_v \tag{13}$$

$$P_V = \left(\frac{NDVI - NDVI_{min}}{NDVI_{max} - NDVI_{min}}\right)^2 \tag{14}$$

$$\epsilon = mP_V + n \tag{15}$$

where ϵ_v and ϵ_s are represented the soil and vegetation emissivity respectively, and F indicates the shape factor ($= 0.55$),

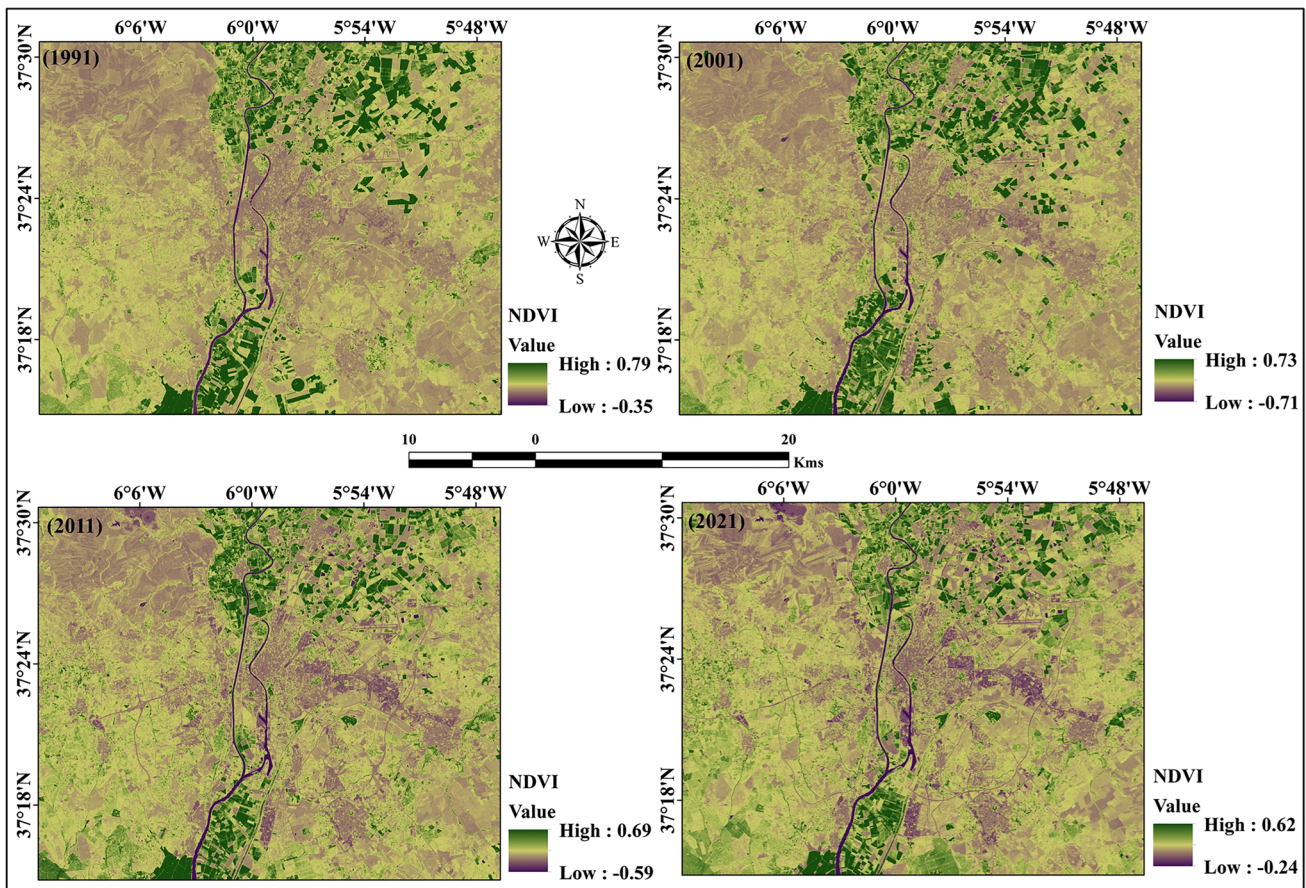


Fig. 7 NDVI maps of the study area

seeing diverse geometric distribution of the satellite data (Sobrino et al. 2004). The values of m and n are considered 0.004 and 0.986 respectively (Sobrino et al. 2004). The NDVI map is prepared using Eq. (4) as mentioned in the previous Sect. 3.4.

The final LST map is prepared by applying Eq. (16) using the satellite brightness temperature (T_B) and surface emissivity (ϵ). (Li et al. 2011; Weng et al. 2004; Estoque & Murayama 2017).

$$LST(^{\circ}C) = \frac{T_B}{1 + (\lambda * T_B / \rho) \ln \epsilon} \quad (16)$$

where, λ is denoted the wavelength of emitted radiance of satellite images, which is measured ($\lambda = 10.8 \mu m$), $\rho = h * c / \sigma$ (1.438×10^{-2} m.K), c indicates velocity of light which is (2.998×10^8 m/s), σ indicates Stefan Boltzmann constant, which is 1.38×10^{-23} J/K, and h is denoted Planck's constant, which is 6.625×10^{-34} J.s; and ϵ represents the surface emissivity of the satellite image.

3.6 Estimation of urban thermal field variance index (UTFVI)

It is not possible to analyze the multi-temporal LST images over an area to estimate the effect of thermal variance on urbanites' health. Instead, a standardized equation is developed based on the LST, known as urban thermal field variance index (UTFVI), which represents the UHI scenarios over an urbanized area. UTFVI maps are investigated using LST data and the following equation is used Eq. (17) (Liu & Zhang 2011; José Antonio Sobrino & Irakulis 2020; Halder et al. 2021b).

$$UTFVI = \left(\frac{LST_{pixel} - LST_{mean}}{LST_{mean}} \right) \quad (17)$$

where, LST_{pixel} indicates the land surface temperature values of the pixels and LST_{mean} indicates the mean LST of the target area. The UTFVI images obtained can be classified into six different levels according to the six different ecological zones such as none, weak, middle, strong, stronger, and strongest, as shown in Table 3.

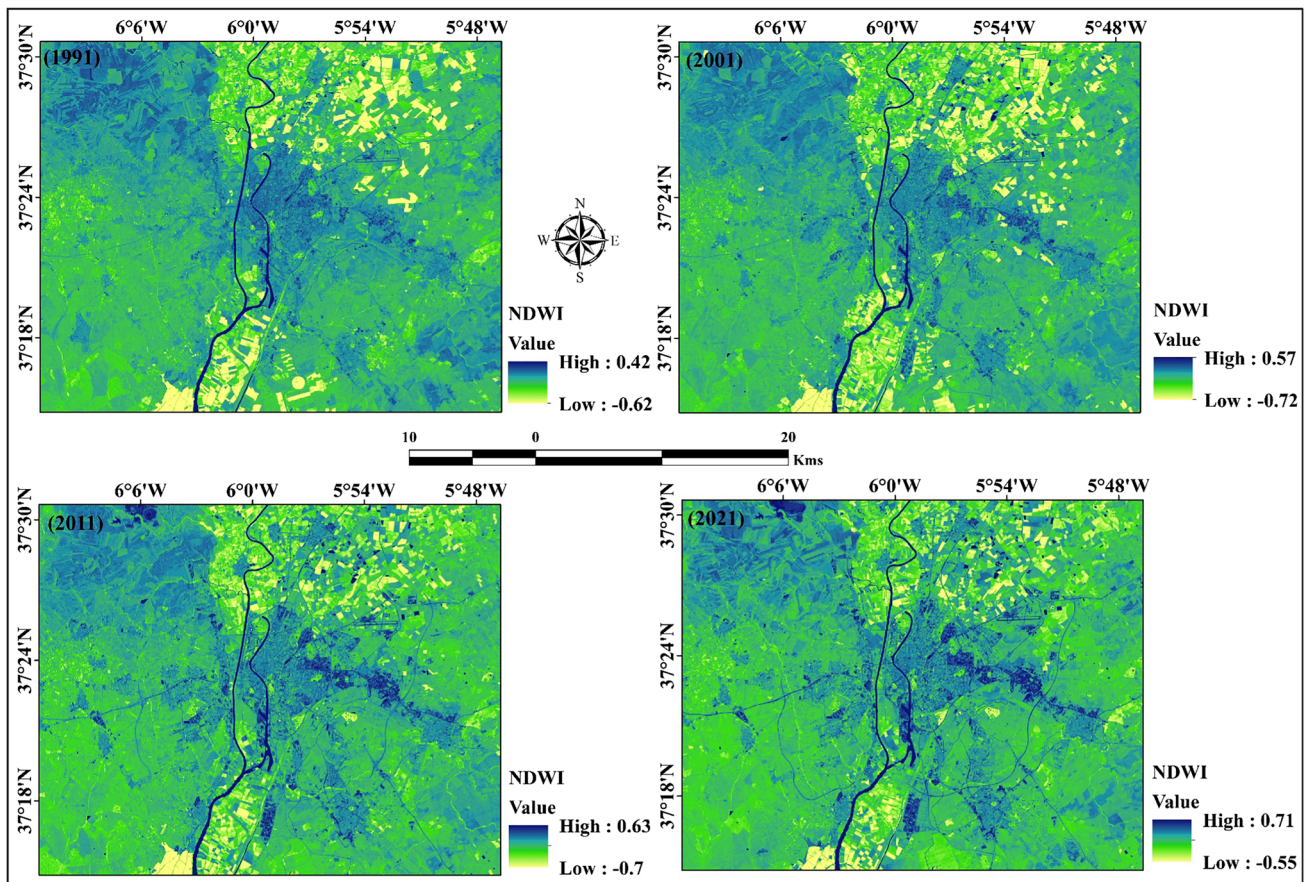


Fig. 8 NDWI maps of the study area

3.7 Urban heat island calculation

The UHI is the key research topic for urban planning and management purpose. Anthropogenic activities and unexpected population pressure are increased the land dynamics and thermal variation (Acero et al. 2013; García & Díaz 2021; García 2022). Vegetation degradation, soil moisture loss, soil erosion, green space dynamics, and air pollution are the results due to unexpected urban expansion. Surface urban heat island (SUHI) and canopy urban heat island (CUHI) are mostly research concern which is identifying the thermal variation and ecological disturbances of the earth's surface (Hu et al. 2019). For the valuation of urban thermal balance, it is essential to estimate the intensity of UHIs (Halder et al. 2021b). LST data from satellite images were used for UHI calculation. The UHI over the Seville city is estimated using the Eq. (18).

$$UHI = \left(\frac{LST_{pixel} - LST_{mean}}{SD} \right) \quad (18)$$

where LST_{pixel} indicates the values of the pixel, LST_{mean} indicates the mean LST of the area in study, and SD indicates the standard deviation of the calculated LST map.

4 Results and discussion

Earth observational remote sensing datasets have been widely used for generating the change of the earth surface and the alteration of the land for several decades (Yu et al. 2014; Kim & Brown 2021). Anthropogenic activities such as urban development, infrastructure development, urban amenities, industrial expansion, and transportation development influence urban climate change scenarios (Owojori & Xie 2005; Cao et al. 2008; Wang et al. 2017; Halder et al. 2021c). Vegetation also influences the heat variation of the earth's surface because overwhelming population pressure and urban expansion are destroying the green portion of the earth's surface, and therefore river water also fluctuated due to water shortage (Tung & Yaseen 2020). This study aimed to identify the effect of urban expansion on information related to UHIs in Seville, Spain (Fig. 3).

4.1 Land alteration study

Land transformation is the most important factor on the surface phenomenon where gradually LULC has been changed

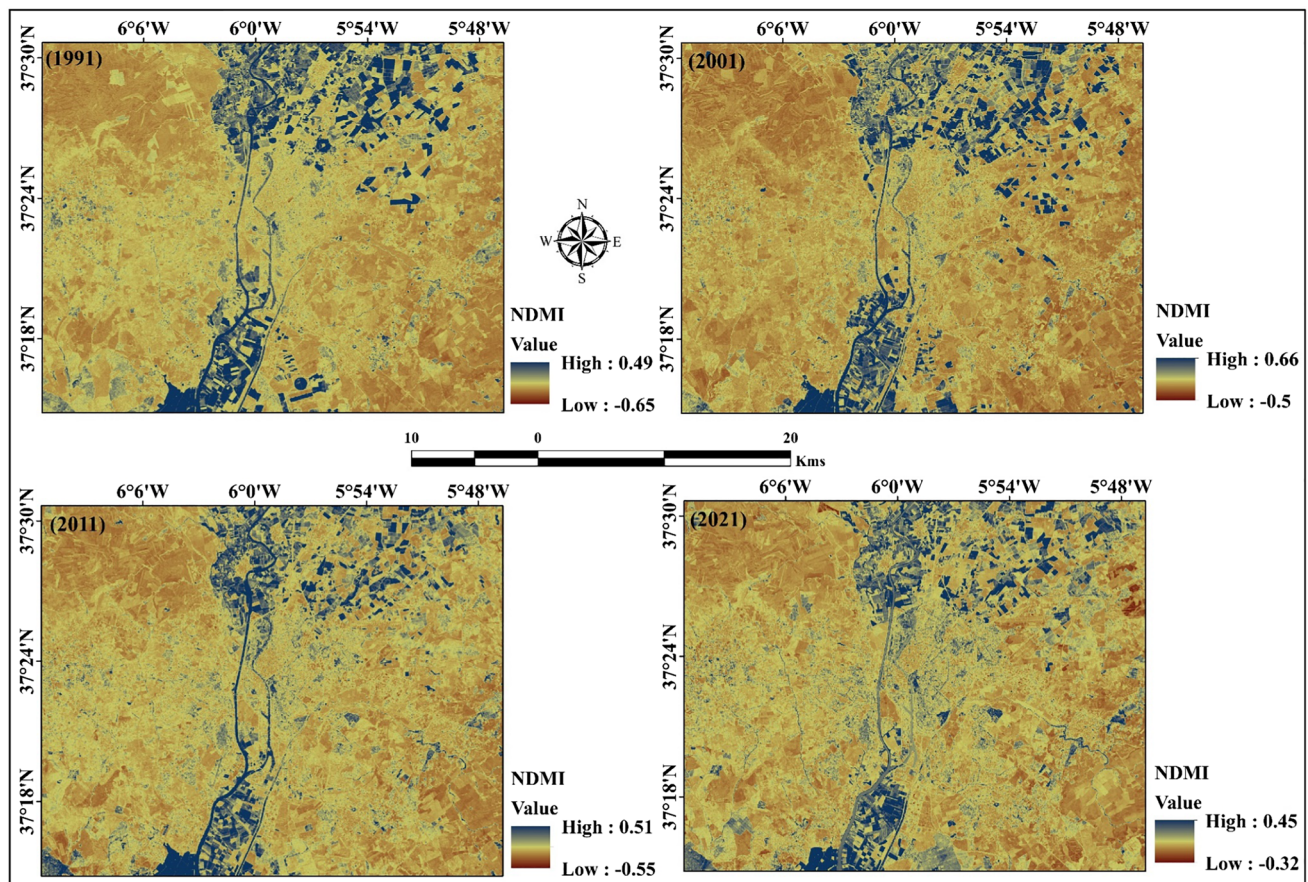


Fig. 9 NDMI maps of the study area

and modified by extreme weather conditions and anthropogenic activities (Corner et al. 2014; Meshesha et al. 2016; Nath et al. 2020). Multi-temporal Landsat 5 (TM) and 8 (OLI/TIRS) data were used to generate the alteration of the city of Seville, where data from four decades, such as 1991, 2001, 2011, and 2021 in the month of July and August, were taken for classification. A supervised classification technique along with a maximum likelihood algorithm was used to define the change in the earth surface in the study area (Singh et al. 2017). Six types of main LULC classes are identified in this study area, such as vegetation, plantation, water bodies, built-up land, open space, and agricultural land, where the mining area is noticed in the years 2001 and 2021.

The total study area is 1447 Km² and the most dominant LULC classes are plantations, open spaces, and agricultural land. Figure 3a to d indicate the LU/LC classification of the study area. The vegetation part of the Seville city area consisted of 107 Km² (1991), 119 Km² (2001), 131 Km² (2011), and 157 Km² (2021). These results show that the vegetation has increased while the plantation area losses due to urban built-up development. The plantation areas are identified as

445 Km² (1991), 479 Km² (2001), 446 Km² (2011), and 414 Km² (2021). Open spaces have gradually decrease due to anthropogenic activities and urban expansion in the Seville city. Table 4 indicates the alteration of the land use classes and the entire LULC diversification classes of the Seville city. The open spaces constituted around 122 Km² (1991), 103 Km² (2001), 101 Km² (2011), and 60 Km² (2021), correspondingly. Most of the open spaces have been converted to agricultural land and built-up land. Figure 3 indicates that open spaces are converted into built-up land in the south, south-eastern, and eastern parts of the Seville city. The open spaces are converted into agricultural land in the north and northwest parts of the Seville city. The plantation areas consist of around 30% of the study area but urban expansion is decreasing the plantation areas along with open spaces and agricultural land. These scenarios indicate that urban expansion influences all regions of the city of Seville.

Water bodies constitute a very small part of the city, yet have been increased gradually. The estimated area is 0.97% (1991), 1.06% (2001), 1.18% (2011), and 1.23% (2021), respectively. The built-up land has also gradually increased from 137 Km² (9.45%) to 165 Km² (11.4%), 193 Km²

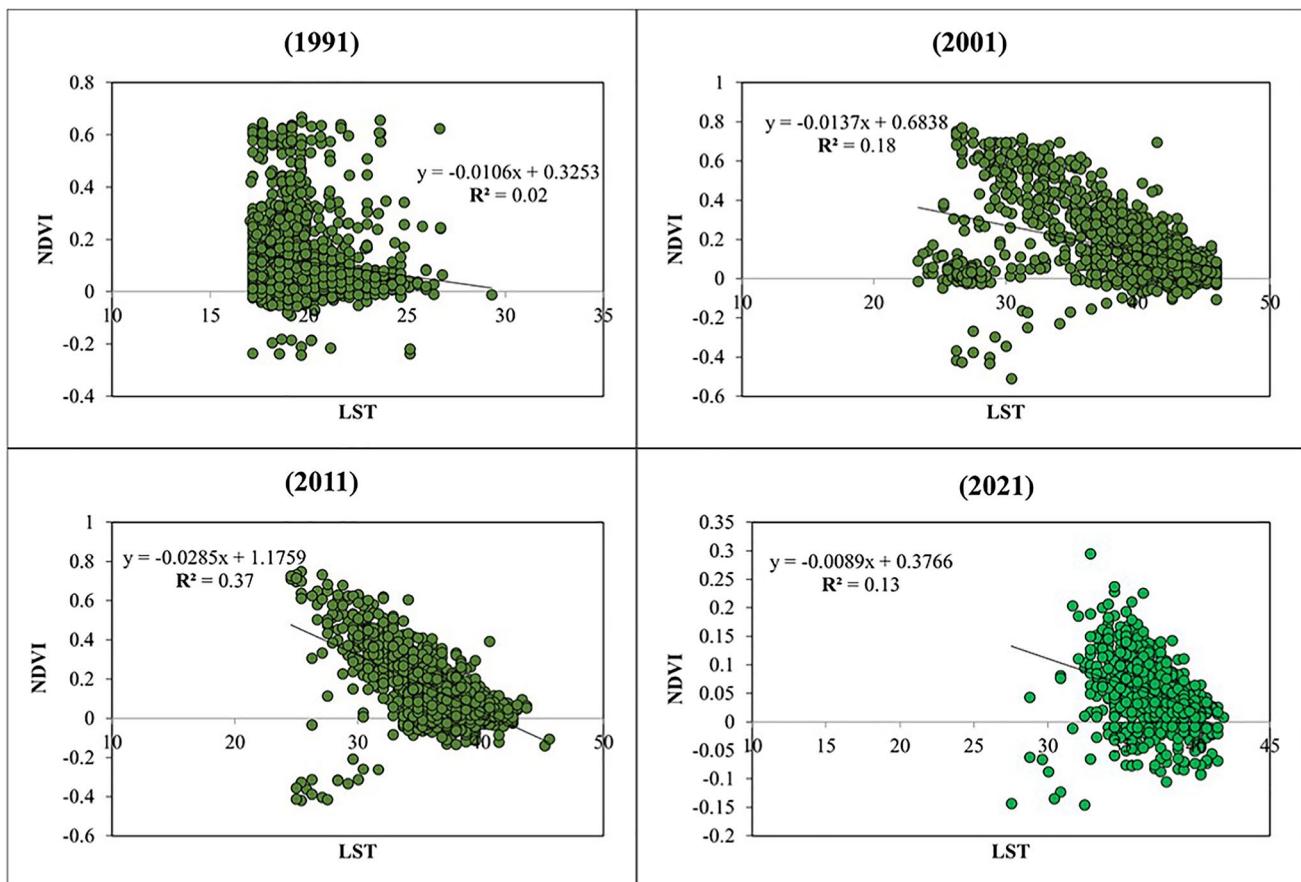


Fig. 10 Correlation analysis of LST and NDVI in different time

(13.37%), and 276 Km² (19.07%) in the year 1991, 2001, 2011, and 2021, respectively. Gradually, agricultural land has decreased from 622 Km² (1991) to 564 Km² (2001), 554 Km² (2011), and 518 Km² (2021), respectively. Agriculture land is decreased in the southeast, south, eastern, and northern parts of the Seville city, where built-up land is extended toward the south, north-eastern, and east parts of the Seville city area.

4.2 LULC change analysis

Table 5 indicates the fluctuation of LULC in the city, where vegetation has increased from 12.4 Km² (1991–2001) to 11.42 Km² (2001–2011), 26.23 Km² (2011–2021), and 50.05 Km² (1991–2021). The most vegetated areas are located in the city area because of thermal comfort and the city area is gradually increasing the vegetation area. Plantation and vegetation areas are lessening due to urban built-up expansion and agricultural development. Figure 4 shows the total area of the different classes and land use and land cover change in the study area. Open spaces have increased from 18.43 Km² (1991–2001) to 22.12 Km² (2001–2011), 41.78 Km² (2011–2021), and 62.33 Km² (1991–2021)

respectively (Fig. 4). Water bodies are increased around 1.33 Km² (1991–2001), 1.69 Km² (2001–2011), 0.81 Km² (2011–2021), and 3.83 Km² (1991–2021), respectively. The built-up areas are increased by 139.2 Km² from 1991 to 2021, where 28.26 Km² (1991–2001), 28.44 Km² (2001–2011), and 82.5 Km² (2011–2021), respectively. Agricultural land also decreased 104.07 Km² in the study periods. These results indicate urban expansion and the causes of UHIs in the study regions. The accuracy assessments of the different years are 76.44%, 79.78%, 79.48%, and 85.10% where kappa coefficients are 0.71, 0.74, 0.75, and 0.81 in the years 1991, 2001, 2011, and 2021, respectively (Tables 6, 7, 8 and 9).

4.3 Distribution of the LST

The LST maps show that the entire Seville city area has an increased thermal variation due to urban expansion, extreme climatic conditions, and other phenomena (Amiri et al. 2009; Sekertekin et al. 2015). The LST maps show that heat alteration and high temperatures located in the four study years. Remote sensing-based Landsat 5 TM (band 6) and Landsat 8 TIRS (band 10) are used to calculate the LST maps of the

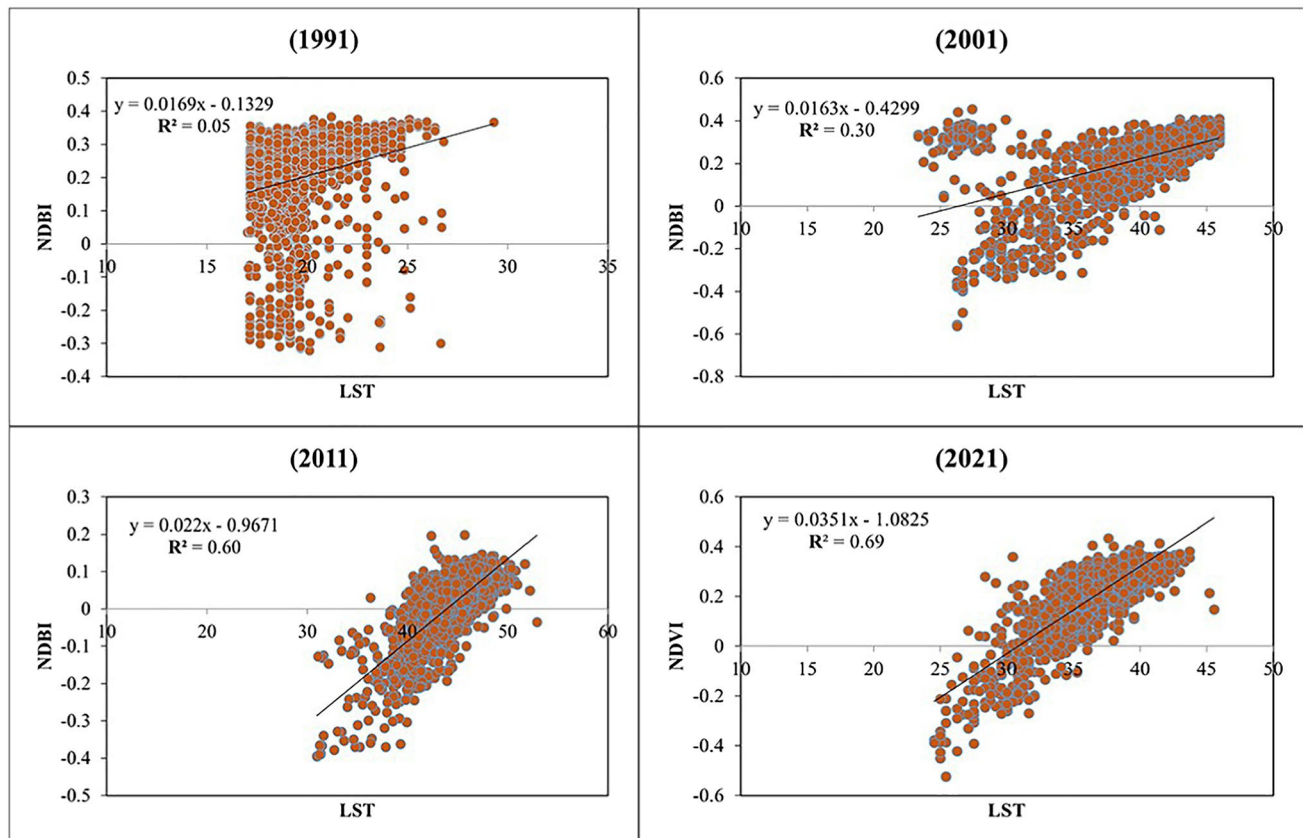


Fig. 11 Correlation analysis of LST and NDBI in different time

study area. Mostly agricultural land and built areas are hotter than the other areas. The high temperatures are located at 30.13 °C (1991), 33.82 °C (2001), 35.85 °C (2011), and 37.11 °C (2021), respectively (Fig. 5). The low temperature also augmented due to global climatic conditions and anthropogenic activities in this area. The average temperature increased around 0.13 °C per year (1991–2021), where the yearly temperature increases 0.37 °C (1991–2001), 0.203 °C (2001–2011), and 0.13 °C (2011–2021), respectively (Fig. 5). This scenario indicates the variation of the LST in the Seville city area. The central parts (urban areas) are observed to have a higher temperature and an increased in the UHI in the Seville city area. The built-up increases and influences the UHI effect and the urban thermal field variation index indicates the ecological disturbances of the study area. Agriculture land increases thermal comfort, but overwhelming population pressure increases UHI values in this study location.

4.4 Identification of geo-spatial indices

In this study, four geospatial indices are used to identify UHI and land alteration studies, such as NDBI, NDVI, NDWI, and NDMI. The built-up expansion index is used to recognize the

built-up scenarios of the Seville city area. The NDBI map values are located high in the Seville city area, but due to the agricultural and plantation area, SWIR bands have a strong influence in that area, so the NDBI values are decreased. Figure 6 indicates the NDBI maps of the study area where the highest values are 0.65 (1991), 0.58 (2001), 0.55 (2011), and 0.32 (2021), respectively (Fig. 6). The NDBI geospatial index is used for monitoring the built-up expansion and the variation of the urban areas on the earth surface where the short-wave infrared (SWIR) and the near-infrared (NIR) bands of satellite data are used. The NDVI maps show that the vegetation areas have decreased in the entire study area. The southern and northern parts are mostly agricultural land and plantations, where the NDVI values are high. The other areas have low NDVI values of different LULC classes. Figure 7 indicates the NDVI maps of the Seville city area in different time periods. The NDVI values are 0.79 (1991), 0.73 (2001), 0.69 (2011), and 0.62 (2021), respectively (Fig. 7). This map shows that vegetation health is reduced due to urban expansion and land alteration in the city of Seville. The green areas indicate healthy vegetation, whereas the bluish locations indicate the built-up land and other LULC classes of the study area.

Figure 8 indicates the NDWI maps of different periods in the NDWI of Seville city, where the values of NDWI are

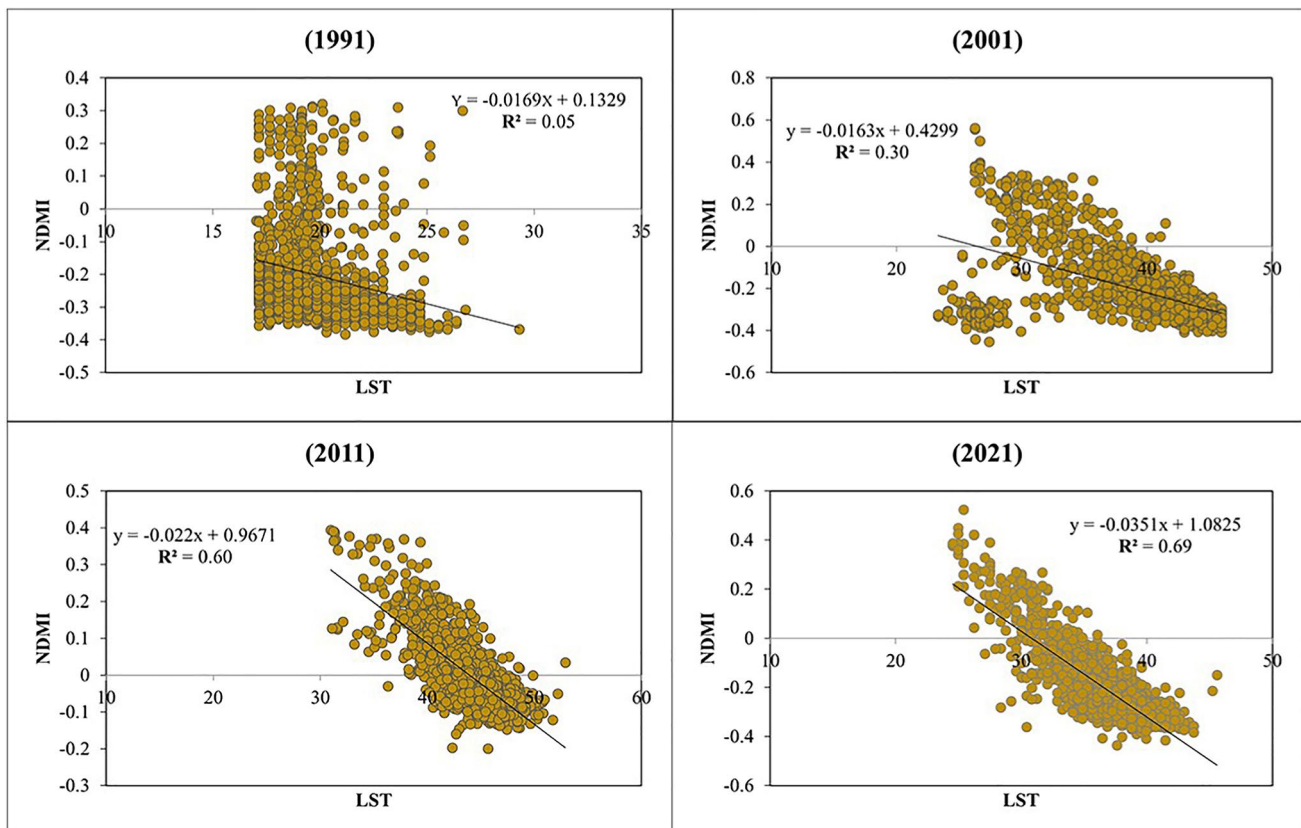


Fig. 12 Correlation analysis of LST and NDMI in different time

gradually increasing due to the development of new lakes, ponds, or water bodies in the Seville city. The NDWI values are located at 0.42 (1991), 0.57 (2001), 0.63 (2011), and 0.71 (2021), respectively (Fig. 8). Those NDWI maps that indicate the water bodies of this area are increasing in different time periods. The northeast parts are located as new water bodies in the study area, where green and near-infrared (NIR) bands are used to estimate the NDWI maps of the study area. Figure 9 indicates the moisture index of the study area. The NDMI index indicates the moisture of the study location where climate change is influencing the location; the brown color denotes the low moisture values and the blue color indicates the high moisture values. Agricultural land, plantations, water bodies, and vegetation areas have high moisture values due to water storage, and built-up land and mining areas are low moisture. The values of NDMI are 0.49 (1991), 0.66 (2001), 0.51 (2011), and 0.45 (2021) respectively (Fig. 9). This map shows that the fluctuation of moisture in the Seville city area indicates the variation of heat, the thermal condition, the urban expansion, and the information related to the heat island. These four indicators are used for the UHI study because the results show that urban expansion and thermal variations impact the study area and the reason for UHI.

4.5 Analysis of the correlation between LST and geospatial indices

Correlation analysis is the most important factor in investigating the thermal variation in different geospatial indices and different time periods. The correlation of LST and different geospatial indices such as NDBI, NDVI, NDWI, and NDMI is denoted as variation and study related to UHI and affected areas in the study area. The correlation of LST and NDVI is located negative relation and the R^2 values are 0.02 (1991), 0.18 (2001), 0.37 (2011), and 0.13 (2021) respectively. This condition indicates that vegetation is decreasing due to urban expansion and anthropogenic activities in the Seville city area (Fig. 10). Figure 11 indicates the positive correlation of LST and NDBI of Seville city, where the R^2 values indicate that LST increases due to urban expansion, climate change, and the alteration of the green land in the study area. The R^2 values are 0.05 (1991), 0.30 (2001), 0.60 (2011), and 0.9 (2021), respectively. This correlation is influenced by the UHI effect in the study area, where the amount of built-up and the LST increased progressively. Figure 12 indicates the correlation of the LST and NDMI values in the city of Seville. The correlation of LST and NDMI is a negative relationship because urban expansion

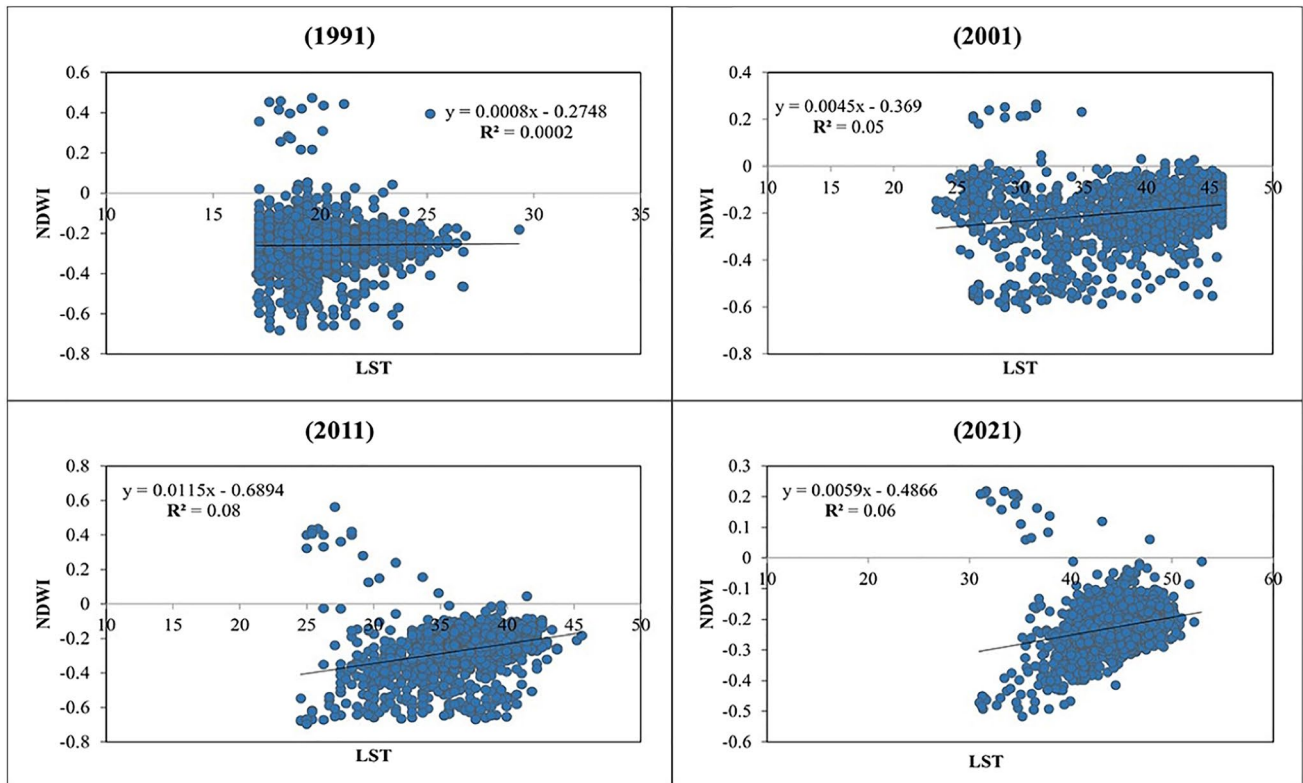


Fig. 13 Correlation analysis of LST and NDWI in different time

and lack of green space influence the moisture of this area. The NDMI and LST correlation are negative, where the R^2 values are 0.05 (1991), 0.30 (2001), 0.60 (2011), and 0.69 (2021), respectively. Figure 13 indicates the correlation between LST and NDWI, where the R^2 values are located at 0.0002 (1991), 0.05 (2001), 0.08 (2011), and 0.06 (2021), respectively. The water bodies are located high in different years, but the LST of the water areas are low, which is why the values are low positive in the study area. This correlation of different geospatial indices and LST is used to investigate the UHI and the ecological study in the study area.

4.6 Urban heat island study

The UHI intensification is a new topic for investigating urban built-up expansion and climate change phenomenon on the earth surface and global climate change (Tolba and Najib 2009; Bucchignani et al. 2018;). The overwhelming population pressure influences the urban green space, thermal variation, surface runoff, and low infiltration rate. Groundwater is also influenced by urban expansion due to the low infiltration rate. Vegetation losses, construction, transportation development, and industrial works have increased in recent times, directly

increasing the UHI effect. Thermal variation and population pressure are pushing the heat island effect (He 2019). Two types of indicators are used to investigate the heat island effect in the city of Seville, such as the urban thermal field variation index (UTFVI) and UHI index. Figure 14 indicates the UTFVI of the study area, where the kelvin LST data and the mean LST data are used to calculate the UTFVI in the study area. This index is used to identify the variation of UTFVI in different time periods in the study area. The highest values are indicating 0.215 (1991), 0.322 (2001), 0.334 (2011), and 0.356 (2021), respectively. This result shows that the UTFVI is gradually increased, indicating ecological disturbances in the study area. The expansion of urban areas is the main reason for the variation of UTFVI in the study area (Fig. 14).

Figure 15 indicates the UHI values of the study area in different time periods. The UHI values are continuously increasing, and the values are 2.21 (1991), 2.89 (2001), 3.29 (2011), and 3.42 (2021), respectively. This result indicates the effect of UHI in Seville city, where urban expansion and low green spaces are the main reason for this variation. The UHI maps indicate the actual scenarios of the study area where urban areas are most affected, and the location of the plantation is high due to the temperature variation in this location. The

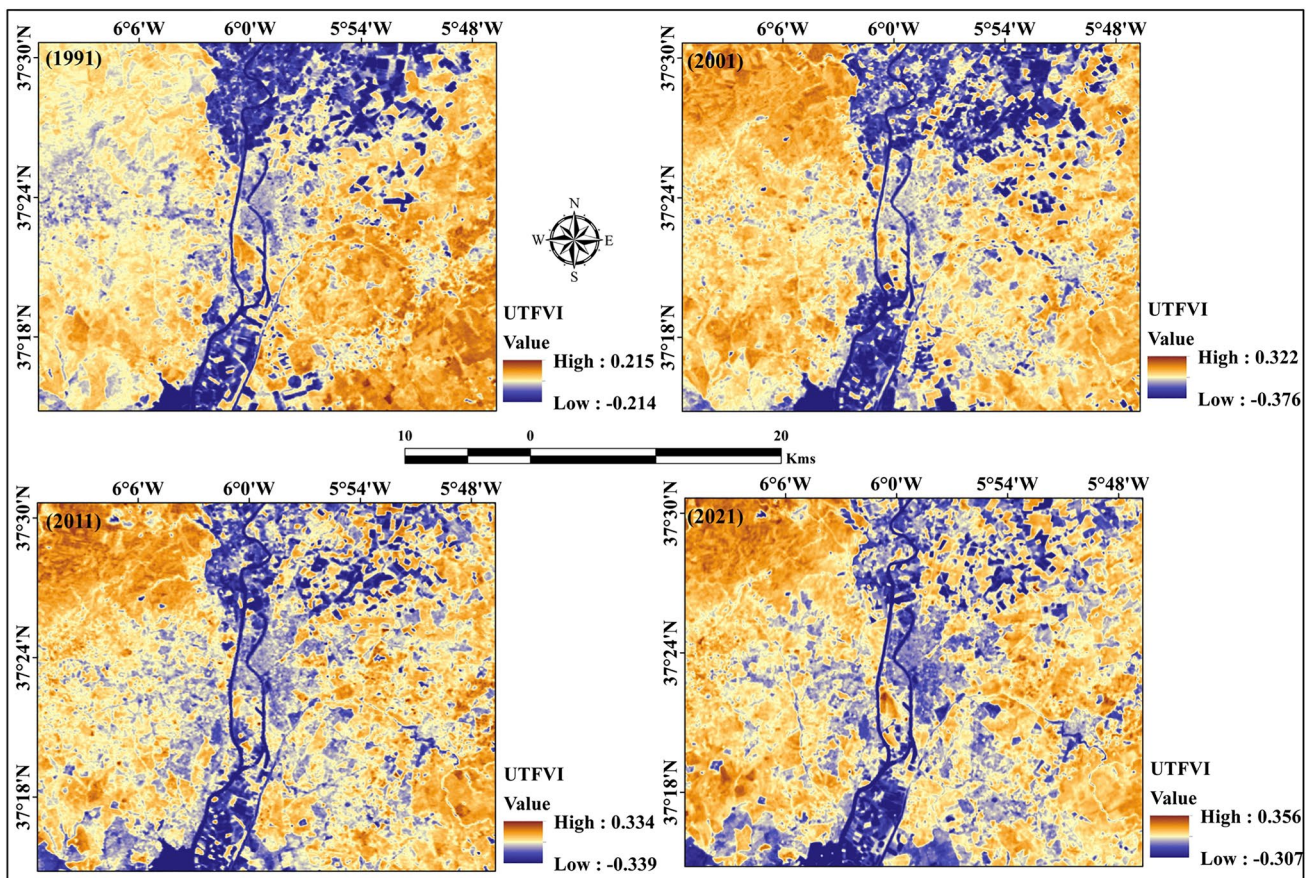


Fig. 14 Urban thermal field variation index (UTFVI) of the study area

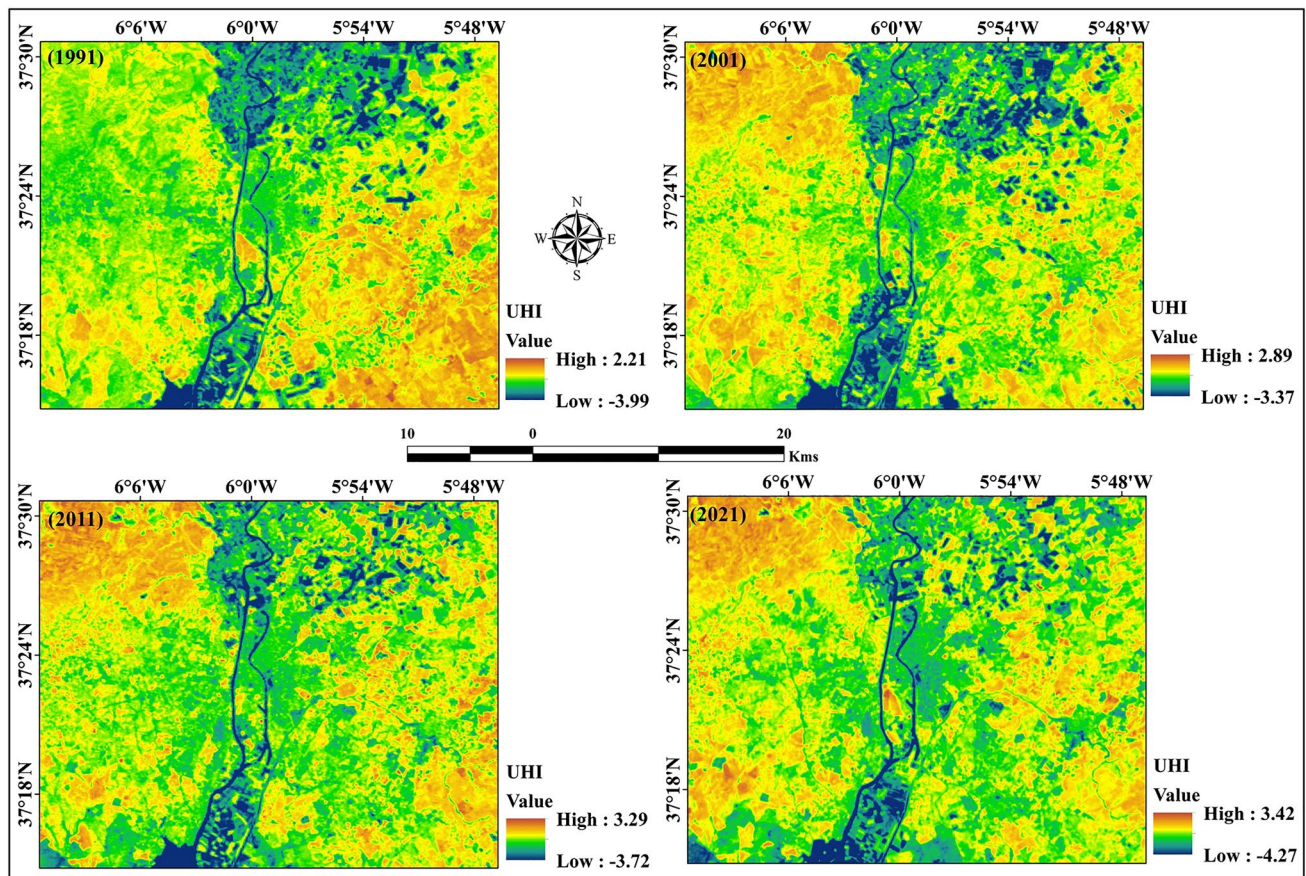


Fig. 15 Urban heat island (UHI) maps of the study area

results of this study are more helpful for the future urban planning, development, and management of the city of Seville.

5 Limitation and recommendation

Remote sensing-based satellite images are widely used for delineating the earth's surface change and environmental degradation related activities. The sensor-based datasets are capturing the thermal variation, LULC change, and land-sea interaction in the earth's surface. The remote sensing-based satellite image analysis and examination are less time taking, cost effective, and accurately observational activities which is increased the earth's surface change visibility. Therefore, those techniques also have some problems or limitation. The satellite images are capturing the data on pixel basis, where urban areas are more heterogeneous due to more feature are notified in a particular region. Proper image classification is more important for farther investigation of the earth's surface change or climatic condition analysis. Sometime, index-based study affected the variation of vegetation or built-up expansion, and therefore pre-processing is the vital concern before investigation. Field survey data is more important

for validation or accuracy assessment of the classification maps. The Seville city is gradually urbanized, and therefore some adaptation policies are necessary to protect the effects of extreme climatic condition, like roof top gardening, plantation, planned urban expansion, awareness to protect the environment, and policy making towards sustainable development of the Seville city. Some future research may be helpful for understanding the other climatic effects on the city like groundwater potential zone, green space dynamics, prediction of future thermal variation or heat alteration, urbanization affected agricultural productivity, water quality analysis in mining area, climatic change, and LULC prediction which are more useful for future research direction and identification of the climatic variation in the Seville city.

6 Conclusions

Urban heat island intensification is the result of overwhelming population pressure and urban expansion. Most of the earth's surface is affected by climate change, whereas arid and semi-arid regions are mostly affected by heat variation. The results of this study investigate land alteration, LST variation,

and information related to UHI in the city of Seville, Spain. The city has gradually developed, and the built-up land has increased by about 139 Km² in just 30 years, while the agricultural land and plantation areas have decreased by around 104 Km² and 31 Km², respectively. The entire region is affected by thermal variation and the UHI has increased by a yearly average of 0.13 °C (1991–2021). The loss of green space is one of the main reasons for the variation in urban heat in the study region. The UHI has affected the area where agricultural land, open spaces, and plantation areas are converted into built-up land, where 62 Km² of open spaces is converted into built-up land and agricultural land. These conditions indicate climate change and anthropogenic activities in the study area, where the built-up areas gradually increase and increase the heat variation in the study regions. The UTFVI is located around 0.141 developed (1991–2021) where the UHI maps indicate that the UHI values are increased 1.21 (1991–2021). These conditions trigger the UHI effect in the study area. Future research is important for this area, such as groundwater potential zone, urban green space, water quality, land subsidence, crop production scenarios, high-rise buildings, and soil erosion. These study results are also helpful to administrators, policy makers, urban planners, researchers, and other stakeholders for sustainable urban planning and development.

Acknowledgements The authors are grateful to the editor and the anonymous reviewers for their valuable and constructive comments and suggestions to improve the quality of the manuscript.

Author contribution Bijay Halder: conceptualization, software, investigation, analysis, validation, project lead, visualization, evaluation, and writing up. Alireza Karimi: conceptualization, investigation, analysis, validation, visualization, evaluation, and writing up. Pir Mohammad: conceptualization, investigation, analysis, validation, visualization, evaluation, and writing up. Jatisankar Bandyopadhyay: supervision, investigation, analysis, visualization, evaluation, and writing up. Robert D Brown: supervision, validation, investigation, analysis, visualization, evaluation, and writing up. Zaher Mundher Yaseen: supervision, validation, investigation, analysis, visualization, evaluation, and writing up.

Data availability Publically available Landsat series of data has been used in this study downloaded from USGS earth explorer website (<https://earthexplorer.usgs.gov/>).

Code availability We did not use any custom coding in the process of producing result shown in this study. Microsoft Excel and ArcGIS software were employed to process all the data and obtain the results and maps.

Declarations

Ethics approval The study is conducted considering the ethical manner advised by the journal.

Consent to participate Not applicable.

Consent for publication All authors approve consent to publish the paper.

Conflict of interest The authors declare no competing interests.

References

- Abulibdeh A (2021) Analysis of urban heat island characteristics and mitigation strategies for eight arid and semi-arid gulf region cities. *Environ Earth Sci* 80:1–26
- Acerro JA, Arrizabalaga J, Kupski S, Katschner L (2013) Urban heat island in a coastal urban area in northern Spain. *Theoret Appl Climatol* 113(1):137–154
- Afsharzadeh M, Khorasanizadeh M, Norouzian-Maleki S, Karimi A (2021) Identifying and prioritizing the design attributes to improve the use of Besat Park of Tehran. *Iran Univ Sci Technol* 31:1–24
- Ali M, Prasad R, Xiang Y, Yaseen ZM (2020) Complete ensemble empirical mode decomposition hybridized with random forest and kernel ridge regression model for monthly rainfall forecasts. *J Hydrol* 584:124647
- Alibakhshi Z, Ahmadi M, Asl MF (2020) Modeling biophysical variables and land surface temperature using the GWR model: case study—Tehran and its satellite cities. *J Indian Soc Remote Sens* 48:59–70
- Amiri R, Weng Q, Alimohammadi A, Alavipanah SK (2009) Spatial–temporal dynamics of land surface temperature in relation to fractional vegetation cover and land use/cover in the Tabriz urban area. *Iran Remote Sens Environ* 113:2606–2617. <https://doi.org/10.1016/j.rse.2009.07.021>
- Armanuos A, Ahmed K, Shiru MS, Jamei M (2021) Impact of increasing pumping discharge on groundwater level in the Nile Delta Aquifer. *Egypt Knowledge-Based Eng Sci* 2:13–23
- Ashrafzadeh MR, Naghipour AA, Haidarian M et al (2019) Effects of climate change on habitat and connectivity for populations of a vulnerable, endemic salamander in Iran. *Glob Ecol Conserv* 19:e00637
- Atasoy M (2020) Assessing the impacts of land-use/land-cover change on the development of urban heat island effects. *Environ Dev Sustain* 22:7547–7557
- Avram S, Onçel I, Negreanu Ş (2019) Impact of land use/land cover on urban heat island (UHI) within bucharest area. *Annals of the University of Craiova. Series Geography/Analele Universitatii din Craiova. Seria Geografie*, 20
- Balçık FB (2014) Determining the impact of urban components on land surface temperature of Istanbul by using remote sensing indices. *Environ Monit Assess* 186:859–872
- Barsi JA, Schott JR, Hook SJ et al (2014) Landsat-8 thermal infrared sensor (TIRS) vicarious radiometric calibration. *Remote Sens* 6:11607–11626. <https://doi.org/10.3390/rs6111607>
- Bayatvarkeshi M, Bhagat SK, Mohammadi K, Kisi O, Farahani M, Hasani A et al (2021) Modeling soil temperature using air temperature features in diverse climatic conditions with complementary machine learning models. *Comput Electron Agric* 185:106158
- Bokaie M, Zarkesh MK, Arasteh PD, Hosseini A (2016) Assessment of urban heat island based on the relationship between land surface temperature and land use/land cover in Tehran. *Sustain Cities Soc* 23:94–104
- Bucchignani E, Mercogliano P, Panitz H-J, Montesarchio M (2018) Climate change projections for the Middle East-North Africa domain with COSMO-CLM at different spatial resolutions. *Adv Clim Chang Res* 9:66–80. <https://doi.org/10.1016/j.accre.2018.01.004>
- Cao L, Li P, Zhang L, Chen T (2008) Remote sensing image-based analysis of the relationship between urban heat island and vegetation fraction. *Int Arch Photogramm Remote Sens Spat Inf Sci* 37:1379–1384

- Castillo-Manzano JJ, López-Valpuesta L, Marchena-Gómez M (2015) Seville: a city with two souls. *Cities* 42:142–151
- Chakraborty T, Hsu A, Many D, Sheriff G (2020) A spatially explicit surface urban heat island database for the United States: characterization, uncertainties, and possible applications. *ISPRS J Photogramm Remote Sens* 168:74–88. <https://doi.org/10.1016/j.isprsjprs.2020.07.021>
- Chatterjee S, Gupta K (2021) Exploring the spatial pattern of urban heat island formation in relation to land transformation: a study on a mining industrial region of West Bengal. *India Remote Sens Appl Soc Environ* 23:100581
- Cohen J (1968) Weighted kappa: nominal scale agreement provision for scaled disagreement or partial credit. *Psychol Bull* 70:213–220. <https://doi.org/10.1037/h0026256>
- Corner RJ, Dewan AM, Chakma S (2014) Monitoring and prediction of land-use and land-cover (LULC) change. In: Dhaka megacity. Springer, Dordrecht, pp 75–97
- Coseo P, Larsen L (2014) How factors of land use/land cover, building configuration, and adjacent heat sources and sinks explain urban heat islands in Chicago. *Landsc Urban Plan* 125:117–129
- Das P, Vamsi KS, Zhenke Z (2020) Decadal variation of the land surface temperatures (LST) and urban heat island (UHI) over Kolkata City projected using MODIS and ERA-interim DataSets. *Aerosol Sci Eng* 4:200–209
- de Medio Ambiente C, del Territorio O (2003) Informe de Medio Ambiente de Andalucía. Junta de Andalucía
- Du J, Xiang X, Zhao B, Zhou H (2020) Impact of urban expansion on land surface temperature in Fuzhou, China using Landsat imagery. *Sustain Cities Soc* 61:102346
- Emran A, Roy S, Bagmar MSH, Mitra C (2018) Assessing topographic controls on vegetation characteristics in Chittagong Hill Tracts (CHT) from remotely sensed data. *Remote Sens Appl Soc Environ* 11:198–208. <https://doi.org/10.1016/j.rsase.2018.07.005>
- Ermida SL, Soares P, Mantas V et al (2020) Google earth engine open-source code for land surface temperature estimation from the landsat series. *Remote Sens* 12:1–21. <https://doi.org/10.3390/RS12091471>
- Estoque RC, Murayama Y (2017) Monitoring surface urban heat island formation in a tropical mountain city using Landsat data (1987–2015). *ISPRS J Photogramm Remote Sens* 133:18–29. <https://doi.org/10.1016/j.isprsjprs.2017.09.008>
- Estoque RC, Murayama Y, Myint SW (2017) Effects of landscape composition and pattern on land surface temperature: an urban heat island study in the megacities of Southeast Asia. *Sci Total Environ* 577:349–359. <https://doi.org/10.1016/j.scitotenv.2016.10.195>
- Falah N, Karimi A, Harandi AT (2020) Urban growth modeling using cellular automata model and AHP (case study: Qazvin city). *Model Earth Syst Environ* 6. <https://doi.org/10.1007/s40808-019-00674-z>
- Fallmann J, Forkel R, Emeis S (2016) Secondary effects of urban heat island mitigation measures on air quality. *Atmos Environ* 125:199–211
- Faqe Ibrahim G (2017) Urban land use land cover changes and their effect on land surface temperature: case study using Dohuk City in the Kurdistan Region of Iraq. *Climate* 5(1):13. <https://doi.org/10.3390/cli5010013>
- Farina A (2012) Exploring the relationship between land surface temperature and vegetation abundance for urban heat island mitigation in Seville, Spain. Luma-Gis Thesis
- Feng H, Zhao X, Chen F, Wu L (2014) Using land use change trajectories to quantify the effects of urbanization on urban heat island. *Adv Sp Res* 53:463–473. <https://doi.org/10.1016/j.asr.2013.11.028>
- Feyisa GL, Dons K, Meilby H (2014) Efficiency of parks in mitigating urban heat island effect: an example from Addis Ababa. *Landsc Urban Plan* 123:87–95
- Gao B-C (1996) NDWI a normalized difference water index for remote sensing of vegetation liquid water from space. *Remote Sens Environ* 58:257–266. <https://doi.org/10.24059/olj.v23i3.1546>
- Galli A, Peruzzi C, Beltrame L et al (2021) Evaluating the infiltration capacity of degraded vs. rehabilitated urban greenspaces: lessons learnt from a real-world Italian case study. *Sci Total Environ* 787:147612
- García DH (2022) Analysis of urban heat island and heat waves using Sentinel-3 images: a study of Andalusian Cities in Spain. *Earth Syst Environ* 6(1):199–219
- García DH, Díaz JA (2021) Modeling of the urban heat island on local climatic zones of a city using Sentinel 3 images: urban determining factors. *Urban Climate* 37:100840
- Gohain KJ, Mohammad P, Goswami A (2021) Assessing the impact of land use land cover changes on land surface temperature over Pune city, India. *Quat Int* 575:259–269
- Goswami A, Mohammad P, Sattar A (2016) A temporal study of Urban Heat Island (UHI)—a evaluation of Ahmedabad city, Gujarat. In: International conference on climate change mitigation and technologies for adaptation, pp 1–5
- Guha S, Govil H, Dey A, Gill N (2018) Analytical study of land surface temperature with NDVI and NDBI using Landsat 8 OLI and TIRS data in Florence and Naples city, Italy. *Eur J Remote Sens* 51:667–678
- Halder B, Bandyopadhyay J, Banik P (2021a) Evaluation of the climate change impact on urban heat island based on land surface temperature and geospatial indicators. *Int J Environ Res*. <https://doi.org/10.1007/s41742-021-00356-8>
- Halder B, Haghbin M, Farooque AA (2021b) An assessment of urban expansion impacts on land transformation of Rajpur-Sonarpur Municipality. *Knowl-Based Eng Sci* 2:34–53
- Halder B, Bandyopadhyay J, Banik P (2021c) Monitoring the effect of urban development on urban heat island based on remote sensing and geo-spatial approach in Kolkata and adjacent areas. *India Sustain Cities Soc* 74:103186
- Halder B, Bandyopadhyay J (2022) Potential sites' selection of ground-water zones using AHP and GIS-based multi-criteria approach of Kolkata Municipal Corporation. *Int J Energy Water Resour*:1–18. <https://doi.org/10.1007/s42108-022-00179-z>
- He BJ (2019) Towards the next generation of green building for urban heat island mitigation: zero UHI impact building. *Sustain Cities Soc*
- Henao JJ, Rendón AM, Salazar JF (2020) Trade-off between urban heat island mitigation and air quality in urban valleys. *Urban Clim* 31:100542
- Herrera-Gomez SS, Quevedo-Nolasco A, Pérez-Urrestarazu L (2017) The role of green roofs in climate change mitigation. A case study in Seville (Spain). *Build Environ* 123:575–584
- Hirano Y, Fujita T (2012) Evaluation of the impact of the urban heat island on residential and commercial energy consumption in Tokyo. *Energy* 37:371–383
- Hu Y, Zhen L, Zhuang D (2019) Assessment of land-use and land-cover change in Guangxi, China. *Scientific Reports* 9(1):1–13
- Ifatimehin OO, Ufuah ME (2006) An analysis of urban expansion and loss of vegetation cover in Lokoja, using GIS techniques. *Zaria Geogr* 17:28–36
- Karimi A, Mohammad P, Gachkar S et al (2021) Surface urban heat island assessment of a cold desert city: a case study over the Isfahan Metropolitan Area of Iran. *Atmos (basel)* 12:1368
- Karimi A, Sanaeian H, Farhadi H, Norouzian-Maleki S (2020) Evaluation of the thermal indices and thermal comfort improvement by different vegetation species and materials in a medium-sized urban park. *Energy Rep* 6:1670–1684. <https://doi.org/10.1016/j.egy.2020.06.015>
- Khaleefa O, Kamel AH (2021) On the evaluation of water quality index: case study of Euphrates River, Iraq. *Knowl-Based Eng Sci* 2:35–43

- Khan F, Das B, Mohammad P (2022) Urban growth modeling and prediction of land use land cover change over Nagpur City, India using cellular automata approach. In: Geospatial technology for landscape and environmental management. Springer, Singapore, pp 261–282
- Kim SW, Brown RD (2021) Urban heat island (UHI) intensity and magnitude estimations: a systematic literature review. *Sci Total Environ* 779:146389
- Kisi O, Heddham S, Yaseen ZM (2019) The implementation of univariable scheme-based air temperature for solar radiation prediction: new development of dynamic evolving neural-fuzzy inference system model. *Appl Energy* 241:184–195
- Kulawardhana R, Welegedara N, Jones K, Crocket D (2021) Effects of land-use/land-cover on urban heat island intensity across metropolitan areas of the conterminous United States. In: AGU Fall Meeting Abstracts, vol 2021, pp GC33C-04
- Lambin EF, Geist HJ (eds) (2008) *Landuse and land-cover change: local processes and global impacts*. Springer Science & Business Media
- Lamine S, Petropoulos GP, Singh SK, Szabó S, Bachari NEI, Srivastava PK, Suman S (2018) Quantifying land use/land cover spatio-temporal landscape pattern dynamics from Hyperion using SVMs classifier and FRAGSTATS®. *Geocarto Int* 33(8):862–878
- Li J, Song C, Cao L et al (2011) Impacts of landscape structure on surface urban heat islands: a case study of Shanghai, China. *Remote Sens Environ* 115:3249–3263. <https://doi.org/10.1016/j.rse.2011.07.008>
- Li X, Zhou Y, Yu S et al (2019) Urban heat island impacts on building energy consumption: a review of approaches and findings. *Energy* 174:407–419
- Liu L, Zhang Y (2011) Urban heat island analysis using the landsat TM data and ASTER data: a case study in Hong Kong. *Remote Sens* 3:1535–1552. <https://doi.org/10.3390/rs3071535>
- Mauree D, Coccolo S, Perera ATD et al (2018) A new framework to evaluate urban design using urban microclimatic modeling in future climatic conditions. *Sustain* 10:1134
- Meftahi M, Monavari M, Kheirkhah Zarkesh M, et al (2022) Achieving sustainable development goals through the study of urban heat island changes and its effective factors using spatio-temporal techniques: the case study (Tehran city). In: *Natural Resources Forum*. Wiley Online Library 88–115
- Mehr AD, Akdegirmen O (2021) Estimation of urban imperviousness and its impacts on flashfloods in Gazipaşa. Turkey. *Knowl Based Eng Sci* 2(1):9–17
- Meshesha TW, Tripathi SK, Khare D (2016) Analyses of land use and land cover change dynamics using GIS and remote sensing during 1984 and 2015 in the Beressa Watershed Northern Central Highland of Ethiopia. *Model Earth Syst Environ* 2:1–12. <https://doi.org/10.1007/s40808-016-0233-4>
- Milesi C, Churkina G (2020) Measuring and monitoring urban impacts on climate change from space. *Remote Sens* 12:3494
- Mohammad P, Aghlmand S, Fadaei A et al (2021) Evaluating the role of the albedo of material and vegetation scenarios along the urban street canyon for improving pedestrian thermal comfort outdoors. *Urban Clim* 40:100993. <https://doi.org/10.1016/j.uclim.2021.100993>
- Mohammad P, Goswami A, Bonafoni S (2019) The impact of the land cover dynamics on surface urban heat island variations in semi-arid cities : a case study in Ahmedabad City, India, using multi-sensor/source data. *Sensors* 19:3701. <https://doi.org/10.3390/s19173701>
- Mohtar WHMW, Maulud KNA, Muhammad NS, Sharil S, Yaseen ZM (2019) Spatial and temporal risk quotient based river assessment for water resources management. *Environ Pollut* 248:133–144
- Mukherjee F, Singh D (2020) Assessing land use–land cover change and its impact on land surface temperature using LANDSAT data: a comparison of two urban areas in India. *Earth Syst Environ* 4:385–407
- Naboni E, Natanian J, Brizzi G et al (2019) A digital workflow to quantify regenerative urban design in the context of a changing climate. *Renew Sustain Energy Rev* 113:109255
- Naganna SR, Beyaztas BH, Bokde N, Armanuos AM (2020) On the evaluation of the gradient tree boosting model for groundwater level forecasting. *Knowl Based Eng Sci* 1(01):48–57
- Nath B, Wang Z, Ge Y et al (2020) Land use and land cover change modeling and future potential landscape risk assessment using Markov-CA model and analytical hierarchy process. *Int J Geo-Inf* 9:134. <https://doi.org/10.3390/ijgi9020134>
- Narimani N, Karimi A, Brown RD (2022) Effects of street orientation and tree species thermal comfort within urban canyons in a hot, dry climate. *Ecol Inform* 69:101671
- Oke TR (1982) The energetic basis of the urban heat island. *Meteorol Soc* 108:1–24
- Owojori A, Xie H (2005) Landsat image-based LULC changes of San Antonio, Texas using advanced atmospheric correction and object-oriented image analysis approaches. In: 5th international symposium on remote sensing of urban areas, Tempe, AZ
- Padmanaban R, Bhowmik AK, Cabral P (2019) Satellite image fusion to detect changing surface permeability and emerging urban heat islands in a fast-growing city. *PLoS ONE* 14:e0208949
- Pauleit S, Ennos R, Golding Y (2005) Modeling the environmental impacts of urban land use and land cover change—a study in Merseyside, UK. *Landscape Urban Plan* 71:295–310
- Phiri D, Morgenroth J (2017) Developments in Landsat land cover classification methods: a review. *Remote Sens* 9:0967. <https://doi.org/10.3390/rs9090967>
- Pramanik S, Punia M (2019) Land use/land cover change and surface urban heat island intensity: source–sink landscape-based study in Delhi, India. *Environ Dev Sustain* 1–26
- Rotem-Mindali O, Michael Y, Helman D, Lensky IM (2015) The role of local land-use on the urban heat island effect of Tel Aviv as assessed from satellite remote sensing. *Appl Geogr* 56:145–153
- Ruiz-Pérez MR, Alba-Rodríguez MD, Rivero-Camacho C, et al (2021) The budget as a basis for ecological management of urbanization projects. Case study in Seville, Spain. *Sustainability* 13:4078
- Saha S, Saha A, Das M et al (2021) Analyzing spatial relationship between land use/land cover (LULC) and land surface temperature (LST) of three urban agglomerations (UAs) of Eastern India. *Remote Sens Appl Soc Environ* 22:100507
- Salman SA, Shahid S, Sharafati A, Ahmed Salem GS, Abu Bakar A, Farooque AA, ..., and Yaseen ZM (2021) Projection of agricultural water stress for climate change scenarios: a regional case study of Iraq. *Agriculture* 11(12):1288
- Sanikhani H, Kisi O, Maroufpoor E, Yaseen ZM (2019) Temperature-based modeling of reference evapotranspiration using several artificial intelligence models: application of different modeling scenarios. *Theor Appl Climatol* 135(1):449–462
- Santos LGR, Nevat I, Pignatta G, Norford LK (2021) Climate-informed decision-making for urban design: assessing the impact of urban morphology on urban heat island. *Urban Clim* 36:100776
- Sarif M, Rimal B, Stork NE (2020) Assessment of changes in land use/land cover and land surface temperatures and their impact on surface urban heat island phenomena in the Kathmandu Valley (1988–2018). *Int J Geo-Information* 9:726
- Sekertekin A, Bonafoni S (2020) Land surface temperature retrieval from Landsat 5, 7, and 8 over rural areas : assessment of different retrieval algorithms and emissivity models and toolbox

- implementation. *Remote Sens* 12:0294. <https://doi.org/10.3390/rs12020294>
- Sekertekin A, Kutoglu SH, Kaya S (2015) Evaluation of spatio-temporal variability in land surface temperature: a case study of Zonguldak, Turkey. *Environ Monit Assess* 188 <https://doi.org/10.1007/s10661-015-5032-2>
- Senay GB, Budde ME, Verdin JP (2011) Enhancing the simplified surface energy balance (SSEB) approach for estimating landscape ET: validation with the METRIC model. *Agric Water Manag* 98:606–618. <https://doi.org/10.1016/j.agwat.2010.10.014>
- Shahmohamadi P, Che-Ani AI, Eteessam I et al (2011) Healthy environment: the need to mitigate urban heat island effects on human health. *Procedia Eng* 20:61–70
- Sharma K (2019) Urbanization induced land use-land cover changes in the Manipur valley and surrounding hills: a landscape metrics approach. In: *Environmental change in the Himalayan Region*. Springer, Cham, pp 137–155
- Singh P, Kikon N, Verma P (2017) Impact of land use change and urbanization on urban heat island in Lucknow city, Central India. A remote sensing based estimate. *Sustain Cities Soc* 32:100–114
- Sobrino JA, Jiménez-Muñoz JC, Paolini L (2004) Land surface temperature retrieval from LANDSAT TM 5. *Remote Sens Environ* 90:434–440. <https://doi.org/10.1016/j.rse.2004.02.003>
- Sobrino JA, Irakulis I (2020) A methodology for comparing the surface urban heat Island in selected urban agglomerations around the world from Sentinel-3 SLSTR data. *Remote Sens* 12:1–31. <https://doi.org/10.3390/RS12122052>
- Talukdar S, Singha P, Mahato S et al (2020) Land-use land-cover classification by machine learning classifiers for satellite observations — a review. *Remote Sens* 12:1135. <https://doi.org/10.3390/rs12071135>
- Tolba MKS, Najib W (2009) Arab environment: climate change: impact of climate change on Arab countries. *Arab Forum for Environment and Development (AFED)*
- Tran DX, Pla F, Latorre-Carmona P et al (2017) Characterizing the relationship between land use land cover change and land surface temperature. *J Photogramm Remote Sens* 124:119–132
- Tung TM, Yaseen ZM (2020) A survey on river water quality modeling using artificial intelligence models: 2000–2020. *J Hydrol* 585:124670
- USGS (2017) Landsat 8 OLI and TIRS calibration notices. [accessed 2022 Jan 24]. Available from: <https://www.usgs.gov/land-resources/nli/landsat/landsat-8-oli-and-tirs-calibration-notice>
- USGS (2019) Landsat 8 (L8) data users handbook. [accessed 2022 Jan 24]. Available from: <https://www.usgs.gov/media/files/landsat-8-data-users-handbook>
- Veena K, Parammasivam KM, Venkatesh TN (2020) Urban heat island studies: current status in India and a comparison with the international studies. *J Earth Syst Sci* 129:1–15
- Wan Z (1996) A generalized split-window algorithm for retrieving land-surface temperature from space. *IEEE Trans Geosci Remote Sens* 34:892–905. <https://doi.org/10.1109/36.508406>
- Wang R, Cai M, Ren C et al (2019) Detecting multi-temporal land cover change and land surface temperature in Pearl River Delta by adopting local climate zone. *Urban Clim* 28:100455
- Wang S, Ma Q, Ding H, Liang H (2018) Detection of urban expansion and land surface temperature change using multi-temporal landsat images. *Resour Conserv Recycl* 128:526–534
- Wang H, Zhang Y, Tsou JY, Li Y (2017) Surface urban heat island analysis of shanghai (China) based on the change of land use and land cover. *Sustain* 9 <https://doi.org/10.3390/su9091538>
- Weng Q (2001) A remote sensing? GIS evaluation of urban expansion and its impact on surface temperature in the Zhujiang Delta, China. *Int J Remote Sens* 22:1999–2014
- Weng Q, Lu D, Schubring J (2004) Estimation of land surface temperature-vegetation abundance relationship for urban heat island studies. *Remote Sens Environ* 89:467–483. <https://doi.org/10.1016/j.rse.2003.11.005>
- Wong NH, Chen Y (2008) *Tropical urban heat islands: climate, buildings and greenery*. Routledge
- Wu H, Ye L-P, Shi W-Z, Clarke KC (2014) Assessing the effects of land use spatial structure on urban heat islands using HJ-1B remote sensing imagery in Wuhan, China. *Int J Appl Earth Obs Geoinf* 32:67–78
- Xu H (2006) Modification of normalised difference water index (NDWI) to enhance open water features in remotely sensed imagery. *Int J Remote Sens* 27:3025–3033
- Yang L, Qian F, Song D-X, Zheng K-J (2016) Research on urban heat-island effect. *Procedia Eng* 169:11–18
- Yu X, Guo X, Wu Z (2014) Land surface temperature retrieval from Landsat 8 TIRS—comparison between radiative transfer equation-based method, split window algorithm and single channel method. *Remote Sens* 6:9829–9852. <https://doi.org/10.3390/rs6109829>
- Zha Y, Gao J, Ni S (2003) Use of normalized difference built-up index in automatically mapping urban areas from TM imagery. *Int J Remote Sens* 24:583–594. <https://doi.org/10.1080/01431160304987>
- Zhao S, Da L, Tang Z et al (2006) Ecological consequences of rapid urban expansion: Shanghai, China. *Front Ecol Environ* 4:341–346

Publisher's note Springer Nature remains neutral with regard to jurisdictional claims in published maps and institutional affiliations.

Springer Nature or its licensor holds exclusive rights to this article under a publishing agreement with the author(s) or other rightsholder(s); author self-archiving of the accepted manuscript version of this article is solely governed by the terms of such publishing agreement and applicable law.